Clean Technologies and Environmental Policy (2020) 22:11–42
https://doi.org/10.1007/s10098-019-01766-1

REVIEW

Recent advancements in visible-light-assisted photocatalytic removal of aqueous pharmaceutical pollutants

Ankush Majumdar[1] · **Anjali Pal**[1]

Received: 10 July 2019 / Accepted: 7 October 2019 / Published online: 17 October 2019

Abstract

Pharmaceuticals are one of the persistent emerging contaminants that are ubiquitous in the aquatic environment due to their extensive application as human and veterinary medicines. The ecotoxicity and microbial resistance are considered to be major adverse environmental and health impact of pharmaceuticals even in trace amounts, which raise global concern. The recalcitrant nature of these pollutants restricts the application of the conventional treatment system for their remediation and triggers extensive research on the various advanced oxidation processes as a promising treatment system. Among them, visible-light-assisted semiconductor photocatalysis has significant potential as an efficient, low-cost, and green technology, which can use even solar energy as a clean and sustainable light source. A comprehensive review on the application of various visible light photocatalysts on the degradation of aqueous pharmaceutical pollutants was attempted to highlight their physiochemical properties, reaction mechanism, and catalytic activity in the laboratory- as well as field-scale operations. The challenges and gaps in the current literature have been identified, and recommendations for prospective research opportunities have been placed based on the findings.

Graphic abstract

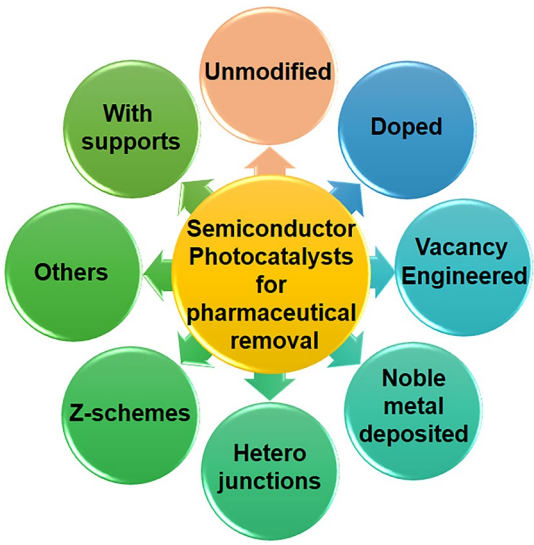

Keywords Photocatalysis · Visible light · Solar light · Pharmaceutical pollutants · Emerging pollutants · Advanced oxidation process

Electronic supplementary material The online version of this article (https://doi.org/10.1007/s10098-019-01766-1) contains supplementary material, which is available to authorized users.

Extended author information available on the last page of the article

Introduction

The water resources of the world are under a constant threat of contamination from both old and new pollutants generated by anthropogenic activities. Speaking of "new pollutants," the term "emerging pollutants" come forward, whose presence and persistence in the aquatic environment even in trace amounts (μg L^{-1} to ng L^{-1}) have caused adverse effects on the environment and health of living organisms. Among these emerging contaminants, many are still unregulated (Rivera-Utrilla et al. 2013). Pharmaceuticals belong to such category of emerging pollutants with adverse environmental and health impacts such as ecotoxicity and microbial resistance. They occur in the aquatic environment due to their widespread applications to protect and improve human and animal health (Halling-Sørensen et al. 1998). Since conventional treatment methods have failed to mitigate the problem of pharmaceutical pollution single-handedly, the removal of pharmaceuticals from the aquatic environment by various advanced technologies gained tremendous research interest very recently (Rivera-Utrilla et al. 2013).

Among the advanced technologies applied for pharmaceutical removal, the semiconductor photocatalysis has been one of the booming research areas, with a study reporting a substantial increase in the number of publications between 2009 and 2017 (Borges et al. 2014; Zhao et al. 2018). Following the breakthrough study of Fujishima and Honda on water splitting by semiconductor photocatalysis (Fujishima and Honda 1972), photocatalysis processes using semiconductors have been extensively applied in various fields, including water splitting (Maeda 2011) and CO_2 reduction (Low et al. 2017) for energy production, water treatment for disinfection (Byrne et al. 2015), and degradation of recalcitrant organic pollutants (Lang et al. 2014). In the era of growing concerns over global energy and environment-related problems, visible-light-assisted photocatalysis is a promising green technology that may use an efficient, low-cost, and eco-friendly photocatalyst and sun as a source of clean and sustainable light energy.

As per the authors' knowledge, reviews on ultraviolet (UV)-based photocatalysis (Serpone et al. 2017), with special focus on TiO_2-based photocatalysts (Kanakaraju et al. 2014; Mahmoud et al. 2017; Awfa et al. 2018) and ZnO-based photocatalysts (Mirzaei et al. 2016), for pharmaceutical removal have been reported. Another review has given insight into the recently developed visible-light-active photocatalysts, broadly toward water treatment with a very tiny focus on pharmaceutical removal (Dong et al. 2015). The present review attempts to fill the gap by covering the progress in the research of visible-light-active photocatalysts aimed toward the removal of aqueous pharmaceutical pollutants, over the decade. The review will systematically introduce its readers to the environmental occurrence, fate, and harmful effects of pharmaceutical pollutants, highlighting the importance of its removal from the aqueous environment. The fundamentals and mechanism of semiconductor photocatalysis are discussed in details. The main focus of the review is on the current development of various unmodified and modified visible-light-active photocatalysts, along with the in-depth understanding of their reaction mechanisms. The role of influential parameters on pharmaceutical removal and the real field applications of the photocatalysts has also been discussed. A brief outlook on the future of visible light photocatalysis for pharmaceutical removal is critically assessed to streamline the research in this area.

A brief overview of pharmaceuticals and their removal technologies

Pharmaceuticals are medicines intended for human and animal use against diseases and to boost growth. The existence of pharmaceuticals was first ascertained in the surface water and groundwater of Europe and the USA in the 1960s. Adverse effects of pharmaceuticals surfaced later in the 1990s with studies conducted on aquatic organisms and their terrestrial consumers (Kyzas et al. 2015). Pharmaceuticals pose a threat to the environment, even at negligibly low concentrations. A constant supply of pharmaceuticals, even with shorter half-lives, is responsible for their pseudo-persistence in the aquatic environment. Pharmaceuticals have diverse nature, chemical structure, usage, dosage, and breakdown process in the human and animal body and the environment (Halling-Sørensen et al. 1998). The use, adverse environmental and health effects, and maximum detected concentrations of pharmaceuticals found ubiquitously in the aquatic environment worldwide are given in Table S1.

Occurrence and fate of pharmaceuticals in the environment

Global production and administration of pharmaceuticals for human and veterinary use amount to thousands of ton per year (Ganiyu et al. 2015). The occurrence of pharmaceuticals in the environment results from their release from different sources such as residences, hospitals, agriculture, aquaculture, and livestock farms (Kummerer 2001). The occurrence and fate of pharmaceuticals in the environment are portrayed in Fig. 1. The consumed pharmaceuticals are not fully metabolized and are excreted by humans and animals in both unmodified (parent pharmaceuticals) and modified (transformed products) forms. Wastewater

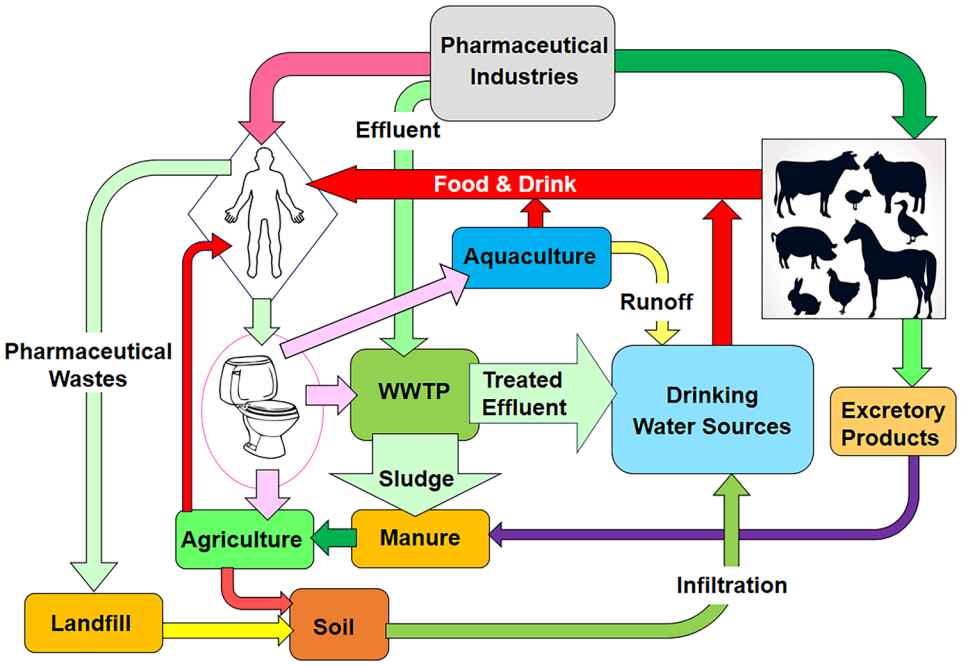

Fig. 1 Occurrence and fate of pharmaceuticals in the environment

treatment plants (WWTPs) receive pharmaceuticals mainly via human excretion, rejected drug disposal (Bound et al. 2006), and untreated pharmaceutical industry effluent (Larsson et al. 2007). It has been reported in many studies that though WWTPs have high removal efficiencies toward the likes of analgesics and anti-inflammatory drugs, the removal efficiency toward therapeutic classes such as antiepileptic, antibiotics, and trimethoprim is very low or nil (Kosma et al. 2014). The WWTP effluent bearing residual pharmaceuticals is discharged into surface waters, while the sludge containing sorbed pharmaceuticals (Kosma et al. 2014) is landfilled or used as manure in agriculture. Pharmaceutical industry wastes are also dumped in municipal solid waste landfills (Larsson 2010). The excretory products of livestock are also used as fertilizers in farming. The pharmaceuticals can run off and leach into surface and groundwater, respectively, from these landfills and farms. As analytical techniques have progressed, the detection of pharmaceuticals occurring at concentrations as low as ng L^{-1} in the environment has been possible. Worldwide, numerous studies have reported their prevalence in different aquatic environments, including surface and groundwater sources used as drinking water supplies (Kosma et al. 2014; Robles-Molina et al. 2014).

Impacts on the environment and human health

Pharmaceuticals are commonly bioactive, recalcitrant, and bio-accumulative in nature. These characteristics are a major cause of harmful effects such as endocrine disruption, reproductive anomalies, development of bacterial resistance, and eco-toxicity even at low concentrations. However, their metabolites can be much more harmful than the parent compound itself. Several studies, including reviews, have reported the toxic behavior of pharmaceuticals toward living organisms (Gunnarsson et al. 2009; Ortiz de García et al. 2014). In addition to being toxic to the environment, heavily used human and veterinary pharmaceutical antibiotics also create bacterial resistance. A study reported the presence of 56,000 resistant genes against almost all classes of antibiotics, including those which mobilize genetic material, in an Indian lake polluted by pharmaceutical industry effluent (Bengtsson-Palme et al. 2014). Antibiotic resistance is not desirable from the viewpoint of human health as human pathogens are provided with resistance genes by environmental bacteria (Martinez 2009). This rapid increase in resistance is one of the prime challenges encountered by the global healthcare sector (Larsson 2010). To develop and implement a monitoring policy, a study selected 40 priority pharmaceuticals including antibiotics, analgesics/anti-inflammatory drugs, antiepileptic/psychiatrics, lipid regulators, β-blockers, and a diuretic along with their metabolites, based on their potential ecotoxicity over a particular region (Besse and Garric 2008). A similar study reported thyroid hormone, analgesic and antihypertensive drugs, antibiotics, antiulcers, bronchodilators, antidiabetics, antidepressants, diuretics, and antiasthmatic among others to be pharmaceuticals of high priority (Dong et al. 2013). Another study claimed that high to medium risk had been posed by a few antibiotics, psychiatric drugs, analgesics–anti-inflammatories, lipid regulators, and beta-blockers (Verlicchi et al. 2012). Moreover, tests with combinations of various pharmaceuticals revealed stronger effects than expected from

the effects measured singly (Cleuvers 2003). Dietrich et al. reported the different toxicological effects of the pharmaceutical mixture on daphnids as compared to the individual pharmaceuticals (Dietrich et al. 2010). The adverse impacts of various selective pharmaceuticals on the environment are summarized in Table S1.

Removal technologies

Although conventional WWTPs are highly efficient in degrading homogeneous biodegradable organic wastes, they struggle against pharmaceuticals, each with unique characteristics. While activated sludge and similar biological processes are ineffective against toxic and recalcitrant pharmaceuticals, physicochemical processes such as coagulation, flocculation, sedimentation, and filtration result in low removal and negligible degradation (Onesios et al. 2009; Verlicchi et al. 2012). The incapability of the WWTPs in handling pharmaceuticals is evident from data summarized from various studies compiled in Table S1, showing the maximum detected concentration of pharmaceuticals from WWTP effluents, among other sources. Studies also reported the ineffective destruction or removal of pharmaceuticals in conventional water treatment plants (Stackelberg et al. 2007; Yang et al. 2017). Thus, employing alternative advanced treatment methods is essential.

Among advanced treatment methods, adsorption, membrane processes, and advanced oxidation processes (AOPs) are popularly used to tackle a wide variety of pollutants present in an aqueous system. Adsorption is an efficient and low-cost method for pharmaceutical removal, but it essentially results in the transfer of the adsorbate from the liquid to the adsorbent, producing a new solid waste with high pharmaceutical concentration (Kyzas et al. 2015; De Andrade et al. 2018). Membrane processes are also effective in pharmaceutical removal, but high operating cost and pressure requirement, membrane fouling, and incapability of handling large volumes are the biggest drawbacks (Homem and Santos 2011). Moreover, this technique also does not degrade the pollutant but concentrates the pollutant onto the membrane.

AOPs are promising methods, categorized into ozone-based, chemical, UV-based, catalytic, electrochemical, and physical processes, generating powerful oxidizing agents (such as $^{\cdot}OH$) capable of degrading and mineralizing pharmaceuticals (Kanakaraju et al. 2018). The electrochemical AOPs, though capable of handling high concentrations of pharmaceuticals, are limited by their applicability to low flow rates and the high cost of reactor operation (Sirés et al. 2014). Although ozone-based AOPs have been effective in degrading many pharmaceuticals barring clofibric acid (CA), diazepam (DZP), and ibuprofen (IBP), high operation costs, low mineralization efficiencies, and formation of toxic intermediates or by-products are major drawbacks (Ikehata et al. 2006). Among UV-based AOPs, UV photolysis yields the lowest degradation efficiency compared to the others that involve a strong oxidizing agent, as the process relies upon irradiation intensity, the sensitivity of the target pharmaceutical, and the quantum yield (Yuan et al. 2009). UV/H_2O_2 and UV/$S_2O_8^{2-}$, in particular, are efficient in degrading pharmaceuticals but cannot be deemed as clean processes due to the use of chemical oxidants (Kanakaraju et al. 2018).

Fenton processes are effective for degrading a wide range of pharmaceuticals (Mirzaei et al. 2017). The homogeneous Fenton systems use iron salts as catalysts and H_2O_2 as the oxidant. They are limited by a narrow pH range of operation to avoid the precipitation of iron oxyhydroxides, and the requirement of an additional treatment step to recover dissolved ions from the treated effluent (Klavarioti et al. 2009). These two drawbacks have been overcome by the heterogeneous Fenton systems (Babuponnusami and Muthukumar 2014). In addition to the stand-alone AOPs, there are reviews of literature highlighting membrane filtration and biological processes combined with the AOPs to obtain greater efficiency in treating pharmaceutical wastewaters (Oller et al. 2011; Ganiyu et al. 2015). A recent review reported a comparative study of energy efficiency of different AOPs and categorized them into three groups based on their electrical energy per order (E_{EO}) values: (1) highly energy efficient (median E_{EO} values < 1 kWh m^{-3}) AOPs such as O_3, O_3/H_2O_2,O_3/UV, UV/H_2O_2, UV/$S_2O_8^{2-}$, UV/Cl_2, and electron beam, (2) medium energy efficient (median E_{EO} values 1–100 kWh m^{-3}) AOPs for instance photo-Fenton, plasma, and electrolytic AOPs, and (3) low energy efficient (median E_{EO} values > 100 kWh m^{-3}) AOPs, for example, UV-based photocatalysis, sonolysis, and microwave-based AOPs (Miklos et al. 2018). Sonolysis and microwave processes are energy demanding and are unsuitable for large-scale applications (Kanakaraju et al. 2018). Although UV-based photocatalysis is falling under the category of energy-consuming process due to the usage of artificial UV light, the visible light photocatalysis, based on sunlight as a renewable source of light energy, is a green and self-sustaining AOP.

There are several reports of the application of visible-light-based semiconductor photocatalysis for efficient degradation and complete mineralization of pharmaceuticals, given in Sect. 3. The detailed mechanism of semiconductor photocatalysis is provided in Sect. 2.4.

Semiconductor photocatalysis

In semiconductor photocatalysis, photon energy ($h\nu$) greater than the bandgap (E_g) of the semiconductor excites an electron (e^-) from the valence band (VB) to the conduction band (CB) generating a hole (h^+) in the VB (Eq. 1).

$$\text{Photocatalyst} + h\nu \rightarrow e^- + h^+ \left(\text{when, } h\nu > E_g\right) \quad (1)$$

After the charge carriers or excitons (e^- and h^+) are separated and transported to the catalyst surface, they participate in the redox reactions with pollutants adsorbed onto the surface of the catalyst. Holes are capable of oxidizing OH^- or H_2O at the surface to produce the powerful oxidant, hydroxyl radicals ($^{\cdot}OH$) (Eq. 2).

$$h^+ + H_2O \rightarrow H^+ + {}^{\cdot}OH \quad (2)$$

$$^{\cdot}OH + \text{pollutant} \rightarrow CO_2 + H_2O \quad (3)$$

$$e^- + O_2 \rightarrow O_2^{\cdot -} \quad (4)$$

$$O_2^{\cdot -} + H^+ \rightarrow {}^{\cdot}HO_2 \quad (5)$$

$$^{\cdot}HO_2 + {}^{\cdot}HO_2 \rightarrow H_2O_2 + O_2 \quad (6)$$

$$H_2O_2 + h\nu \rightarrow 2\,{}^{\cdot}OH \quad (7)$$

$$O_2^{\cdot -} + \text{pollutant} \rightarrow CO_2 + H_2O \quad (8)$$

$$^{\cdot}HO_2 + \text{pollutant} \rightarrow CO_2 + H_2O \quad (9)$$

Oxygen adsorbed on the surface of the catalyst is reduced to form superoxide radicals ($O_2^{\cdot -}$) by the e^- in the CB (Eq. 4), which may subsequently react with H^+ to generate hydroperoxyl radical ($^{\cdot}HO_2$) (Eq. 5), further yielding hydrogen peroxide (H_2O_2) by electrochemical reduction (Eq. 6). H_2O_2 is further decomposed by light to generate $^{\cdot}OH$ (Eq. 7). The formed reactive oxygen species (ROS), viz. $^{\cdot}OH$, $O_2^{\cdot -}$, $^{\cdot}HO_2$, and H_2O_2, can degrade and mineralize recalcitrant organic pollutants to harmless end products such as CO_2 and H_2O (Eqs. 3, 8, 9) (Pelaez et al. 2012). Furthermore, the photogenerated h^+ is also regarded as an oxidant to degrade organic pollutants directly to some extent, depending upon the reaction conditions and type of catalyst used (Dong et al. 2015). Finally, the e^-–h^+ pairs recombine on the catalyst surface or in the bulk medium producing light or heat. A schematic representation of the mechanism of semiconductor photocatalysis toward organic pollutant degradation is shown in Fig. 2a.

The efficiency of the photocatalyst depends on three essential factors: (1) bandgap energy (E_g): Photocatalyst with wide bandgap is UV light sensitive and photocatalyst with narrow bandgap is visible light sensitive; (2) band edge potentials, i.e., the potentials of VB and CB: The ROS can

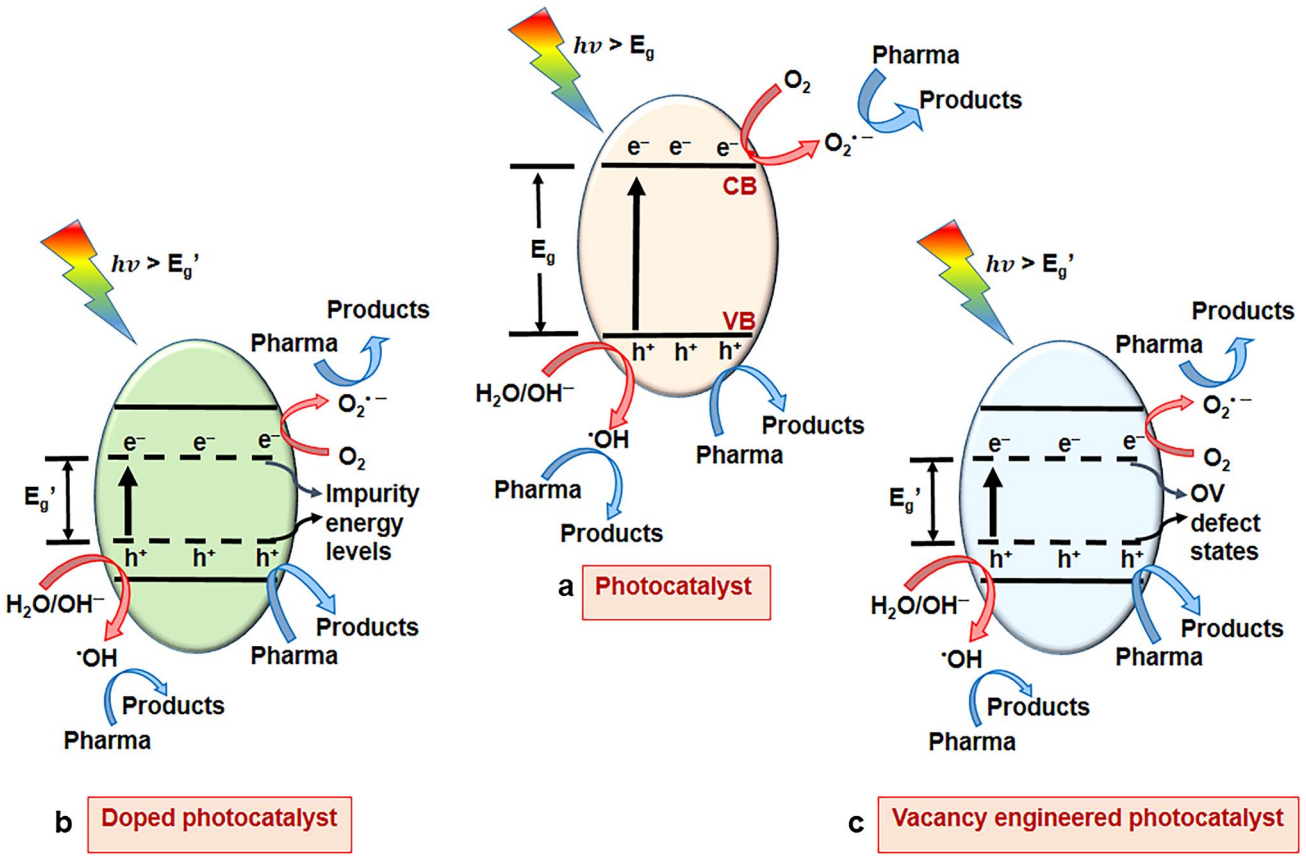

Fig. 2 Mechanism of visible-light-assisted pharmaceutical degradation by **a** semiconductor photocatalyst, **b** doped photocatalyst, and **c** vacancy engineered photocatalyst

only be generated when the CB potential is more negative than reduction potential of O_2 to $O_2^{\cdot-}$ (−0.33 eV vs. NHE) and/or VB potential is more positive than standard oxidation potential of $^{\cdot}OH/H_2O$ (+2.68 eV vs. NHE) or $^{\cdot}OH/OH^-$ (+1.99 eV vs. NHE) (Panneri et al. 2017). If that is not the case, then the h^+ in the VB reacts with the pollutant directly. The more ROS generated, the more is the efficiency of the semiconductor; and (3) rate of recombination of e^-–h^+ pairs: Recombination of e^-–h^+ pairs, owing to the strong Coulombic attraction between them, also reduces the catalyst efficiency. Recombination causes the e^- to turn back to the VB without performing the reduction reaction to form $O_2^{\cdot-}$ (Pelaez et al. 2012). Thus, the choice of the photocatalyst should be made considering these three important factors.

Visible light photocatalysts for removal of pharmaceuticals

Numerous wide-bandgap semiconductors such as TiO_2 and ZnO have been reported to be used as photocatalysts for the degradation of a wide variety of organic pollutants including pharmaceuticals (Chong et al. 2010; Omorogie and Ofomaja 2017). Good chemical stability, low cost, eco-friendly nature, and remarkable electronic and optical properties have made TiO_2 the most prevalent among the other semiconductors (Gaya and Abdullah 2008). Various studies have reported the photodegradation of a wide range of pharmaceuticals present in different aqueous matrices by TiO_2 under UV light (Zhu et al. 2013; Safari et al. 2014). Palominos et al. used both TiO_2 and ZnO for complete degradation and effective mineralization of tetracycline (TC) under simulated solar light (Palominos et al. 2009). Another study using photocatalyst TiO_2 was performed under simulated solar light in which oxytetracycline (OTC) was completely degraded (Pereira et al. 2011). However, these wide-bandgap photocatalysts have fast charge recombination rates and are sensitive only to UV light (high *hv*), which is merely 4–5% of the solar spectrum, making them an impractical choice for large-scale applications. From this viewpoint, the narrow bandgap photocatalysts, sensitive to visible light (low *hv*), that make up about 52% of the solar spectrum, seem to be a greener and more sustainable solution toward the degradation of recalcitrant organic pollutants.

Unmodified semiconductor photocatalysts

Among visible light photocatalysts, graphitic carbon nitride (g-C_3N_4) is a popular metal-free narrow bandgap (2.7 eV) semiconductor, which is easy to prepare, has high chemical stability, and has efficient visible light response. Hernández-Uresti et al. have successfully used g-C_3N_4 in the photodegradation of TC and ciprofloxacin (CIP) in aqueous solution under UV–visible irradiation (Hernández-Uresti et al. 2016). The VB potential of g-C_3N_4 (+1.57 eV vs. SHE) is more negative than the standard redox potentials of $^{\cdot}OH/H_2O$ and $^{\cdot}OH/OH$, which restricts the generation of $^{\cdot}OH$ (Hong et al. 2016). The rapid recombination of photogenerated e^-–h^+ pairs is also a major limitation of pure g-C_3N_4 as a photocatalyst (Xue et al. 2015a). Sturini et al. studied the simulated solar-light-assisted degradation of ofloxacin (OFL) present in tap water and river water by g-C_3N_4 (Sturini et al. 2017). However, a high rate of photo-excited charge carrier recombination is a major limitation of pure g-C_3N_4.

Semiconductors, for instance, bismuth oxyhalides (BiOX, X = F, Br, Cl and I), have become much popular visible-light-active photocatalyst due to their narrow bandgap and low e^-–h^+ recombination resulting from a distinctive layered structure with an internal static electric field sandwiched between each layer (Hao et al. 2012). BiOI has the smallest bandgap (~1.85 eV) with high surface-to-volume ratio and anti-aggregation properties, making it highly effective as a photocatalyst. Hao et al. synthesized mesoporous BiOI microspheres for adsorption and subsequent degradation and mineralization of tetracycline hydrochloride (TCH) (Hao et al. 2012). Another study reported the photocatalytic degradation of IBP by BiOBr microspheres (Li et al. 2016b). Xiao et al. reported that stable, hierarchical $Bi_{24}O_{31}Br_{10}$ nanoflakes with a bandgap of 2.51 eV, larger surface area, and negatively charged surface, exhibited higher efficiency than hierarchical BiOBr microspheres for TCH degradation in real wastewater (Xiao et al. 2013). Hierarchically structured materials possess multiple morphologies and structures and exhibit enhanced photocatalytic performance. Hierarchical BiOCl microspheres were used as a photocatalyst for carbamazepine (CBZ) degradation using a solar light simulator (Gao et al. 2015).

Bismuth-based transition metal oxides have also been reported as good visible light photocatalysts in the degradation of pharmaceuticals. Successful photocatalytic degradation of IBP was reported using $BiVO_4$, which has a narrow bandgap (E_g ~2.4 eV) and chemical stability, but poor e^-–h^+ pair separation (Li et al. 2016a). Xue et al. have used $BiFeO_3$ with a bandgap of 1.97 eV, as a visible light photocatalyst for the degradation of TC (Xue et al. 2015b). Studies have reported the efficient degradation of norfloxacin (NOR) and TC in water under simulated solar light irradiation using Bi_2WO_6, a layered perovskite, which can inhibit e^-–h^+ pair recombination (Chen and Chu 2015; Chu et al. 2016). The layered structure of the perovskites supports efficient charge carrier separation. Hailili et al. synthesized a 3D hierarchically nano-structured $Bi_5FeTi_3O_{15}$ perovskite for photocatalytic degradation of TC (Hailili et al. 2017). The charge transfer efficiency between Fe^{3+} and Ti^{4+} and also between the individual layers, the extended light absorption range due to the formation of a hybridized VB by the presence

of Bi and Fe, which also allows fast hole transfer, magnetic property aided by Fe, everything contributes to this highly efficient photocatalyst. Furthermore, the best photocatalytic efficiency obtained from the 3D nanoflower-like morphology over other morphologies provides an insight into the effects of morphological changes on the change in photodegradation efficiency.

Transition metal sulfides have shown great visible light photocatalytic efficiency and photochemical corrosion resistance. Ai et al. used In_2S_3, with a bandgap of ~ 2.3 eV for photocatalytic degradation of TC under natural sunlight (Ai et al. 2015). Another study reported $ZnIn_2S_4$ photocatalyst for visible light degradation of CBZ (Bo et al. 2017).

For efficient visible-light-induced photocatalysis, the semiconductors should possess narrow band gaps, diminished charge recombination rates, and strong redox ability. However, a single photocatalyst simultaneously exhibiting good visible light response and high redox ability is not feasible. To achieve strong redox ability for ROS forming reactions to occur, the bandgap of a single photocatalyst must be large enough to ensure that the respective bandgap edge is sufficiently more negative than the reduction potential of $O_2^{\cdot-}/O_2$ and more positive than the oxidation potential of $^{\cdot}OH/H_2O$ simultaneously. A photocatalyst with a large bandgap will be unable to use the visible light. Various modification strategies must be undertaken to overcome these constraints and enhance the photocatalytic efficiency. The efficiency of unmodified semiconductor photocatalysts for the degradation of pharmaceuticals is presented in Table 1, along with their detailed reaction conditions.

Semiconductor photocatalysts doped with metals and nonmetals

Doping wide-bandgap photocatalysts with metals (Sr, Bi, Fe, etc.) and nonmetals (C, N, S, B, etc.) can narrow its bandgap by creating impurity energy levels within the bandgap, to utilize visible light and also to enhance e^-–h^+ separation. Optimal content of the dopant serves as electron traps to suppress the e^-–h^+ recombination (Jesudoss et al. 2016), while an excess dopant would facilitate charge recombination (Wang et al. 2011a). A schematic of the mechanism for visible-light-mediated pharmaceutical degradation by doped photocatalysts is presented in Fig. 2b.

An example of the nonmetal-doped visible-light-active photocatalyst is TiO_2 tri-doped with the optimum amount of C–N–S that has been successfully used for TC degradation (Wang et al. 2011a). The tri-doping was instrumental in narrowing the bandgap to expand the light-harvesting capacity of the photocatalyst, while the excited carbonaceous species acting as a photosensitizer, injected e^- into the CB of the photocatalyst. Similarly, Wang et al. developed a C-sensitized and N-doped TiO_2 for photocatalytic degradation of sulfanilamide (SNM) (Wang et al. 2011b). Panneri et al. synthesized a C-doped g-C_3N_4 photocatalyst by an aqueous spray drying process, as given in Fig. 3a, and reported the solar-light-assisted degradation of TC (Panneri et al. 2017). Sheets of g-C_3N_4 are spray-dried using polyvinyl alcohol as a binder to create g-C_3N_4 microsphere (Fig. 3b), which retains its spherical morphology after calcination and thermal oxidation etching processes to produce C-doped g-C_3N_4 (Fig. 3c). Compared to pure g-C_3N_4, C-doping changes both the band edge potentials of g-C_3N_4 to narrow down the bandgap (Fig. 3d) and reduces e^-–h^+ recombination (Fig. 3e), thus improving the visible light activity. Spiramycin (SP) was degraded using N-doped TiO_2 photocatalyst in a study (Vaiano et al. 2015). Simsek used B-doped TiO_2 photocatalysts to degrade IBP and flurbiprofen (FLU) (Bilgin Simsek 2017).

One of the many examples of metal-doped semiconductor photocatalyst is a Sr-doped β-Bi_2O_3 photocatalyst that has been used for the degradation of TC (Niu et al. 2013). Strontium titanate ($SrTiO_3$) is a wide-bandgap ($E_g = 3.2$ eV) semiconductor photocatalyst that is only responsive to UV light and has good photochemical stability and biocompatibility. Li et al. reported that Fe^{3+}-doped $SrTiO_3$ showed excellent degradation of TC (Li et al. 2014). Electrons are transferred to the CB from an impurity energy level created by the dopant near the VB edge, which narrows down the bandgap. Similarly, Cai et al. and Wu et al., respectively, found that Cr- and Mn-doped $SrTiO_3$ to be efficient photocatalysts for TC degradation (Cai et al. 2015; Wu et al. 2015). Ding et al. reported the Bi^{3+} self-doped $NaBiO_3$ photocatalyst for the degradation and mineralization of CBZ (Ding et al. 2017). Another study reported Cu-doped TiO_2 photocatalyst for paracetamol (PAR) degradation (Lin and Yang 2013). The efficiency of doped photocatalysts and their operating conditions for visible-light-assisted degradation of pharmaceuticals is given in Table 2.

Vacancy engineered photocatalysts

The influence of surface and crystal structures on the physicochemical properties of a semiconductor is profuse. Defects, such as vacancies, introduce new energy levels in the band structure of the semiconductors and help reduce the bandgap energy. This reduction in bandgap broadens the light-harvesting range of the semiconductor. Oxygen vacancy (OV) is one such crystal defect in a semiconductor that forms OV state, i.e., a new energy level between VB and CB, which narrows the bandgap of the semiconductor and makes it visible light responsive (Yu et al. 2018). OV also acts as a photogenerated charge-trapping site to increase e^-–h^+ pair separation (Hailili et al. 2018). The mechanism of visible light photocatalysis of pharmaceuticals by vacancy engineered photocatalysts is presented in Fig. 2c.

Table 1 Efficiency of unmodified semiconductor photocatalysts for degradation of pharmaceuticals and their operating conditions

Photocatalyst	Pharmaceutical	Operating conditions	Degradation efficiency/time (min)	Mineralization efficiency/time (min)	k_{app} (min^{-1})	References
$Bi_5FeTi_3O_{15}$	TC	TC: 4.45 mg L^{-1} Catalyst: 0.4 g L^{-1} 300 W Xe lamp with 420-nm cutoff filter	99.34%/60	93.21%/60	0.197	Hailili et al. (2017)
BiOBr	IBP	IBP: 10.31 mg L^{-1} Catalyst: 1 g L^{-1} 500 W Xe lamp with UV cutoff filter pH: 4–9	80%/120	63%/120	–	Li et al. (2016b)
BiOCl	CBZ	CBZ: 2.5 mg L^{-1} Catalyst: 0.5 g L^{-1} 350 W Xe lamp Solar simulator pH: 9	100%/150	–	0.0237	Gao et al. (2015)
$ZnIn_2S_4$	CBZ	CBZ: 0.1 mg L^{-1} Catalyst: 0.03 g L^{-1} 100 W I-Ga lamp pH: 9	100%/20	–	–	Bo et al. (2017)
$BiVO_4$	IBP	IBP: 10 mg L^{-1} Catalyst: 5 g L^{-1} 350 W Xe lamp pH: 4.5	90%/25	–	–	Li et al. (2016a)
g-C_3N_4	TC CIP	TC: 20 mg L^{-1} CIP: 10 mg L^{-1} Catalyst: 1 g L^{-1} 35 W Xe lamp Solar simulator	TC: 86%/240 CIP: 60%/240	TC: > 80%/2880 CIP: > 50%/2880	TC: 0.005 CIP: 0.0024	Hernández-Uresti et al. (2016)
g-C_3N_4	OFL	OFL: 10 mg L^{-1} Catalyst: 0.5 g L^{-1} Solar simulator pH: 7.7	100%/10	–	0.49	Sturini et al. (2017)
Bi_2WO_6	TC	TC: 20 mg L^{-1} Catalyst: 0.5 g L^{-1} 350 W Xe lamp Solar simulator	97%/120	31%/360	0.0139	Chu et al. (2016)
Bi_2WO_6	NOR	NOR: 10 mg L^{-1} Catalyst: 0.5 g L^{-1} 300 W Xe lamp Solar simulator	83.7%/20	–	0.087	Chen and Chu (2015)
In_2S_3	TC	TC: 20 mg L^{-1} Catalyst: 2.5 g L^{-1} Sunlight pH: 7	100%/40	–	–	Ai et al. (2015)
$BiFeO_3$	TC	TC: 10 mg L^{-1} Catalyst: 0.5 g L^{-1} Visible light pH: 8	78%/120	19%/120	0.012	Xue et al. (2015b)
BiOI	TCH	TCH: 40 mg L^{-1} Catalyst: 1 g L^{-1} 1000 W Xe lamp with 420-nm cutoff filter	94%/120	72.58%/240	–	Hao et al. (2012)
$Bi_{24}O_{31}Br_{10}$ nanoflakes	TC	TC: 40 mg L^{-1} Catalyst: 1 g L^{-1} 1000 W Xe lamp with 420-nm cutoff filter	94%/60	70.9%/60	–	Xiao et al. (2013)

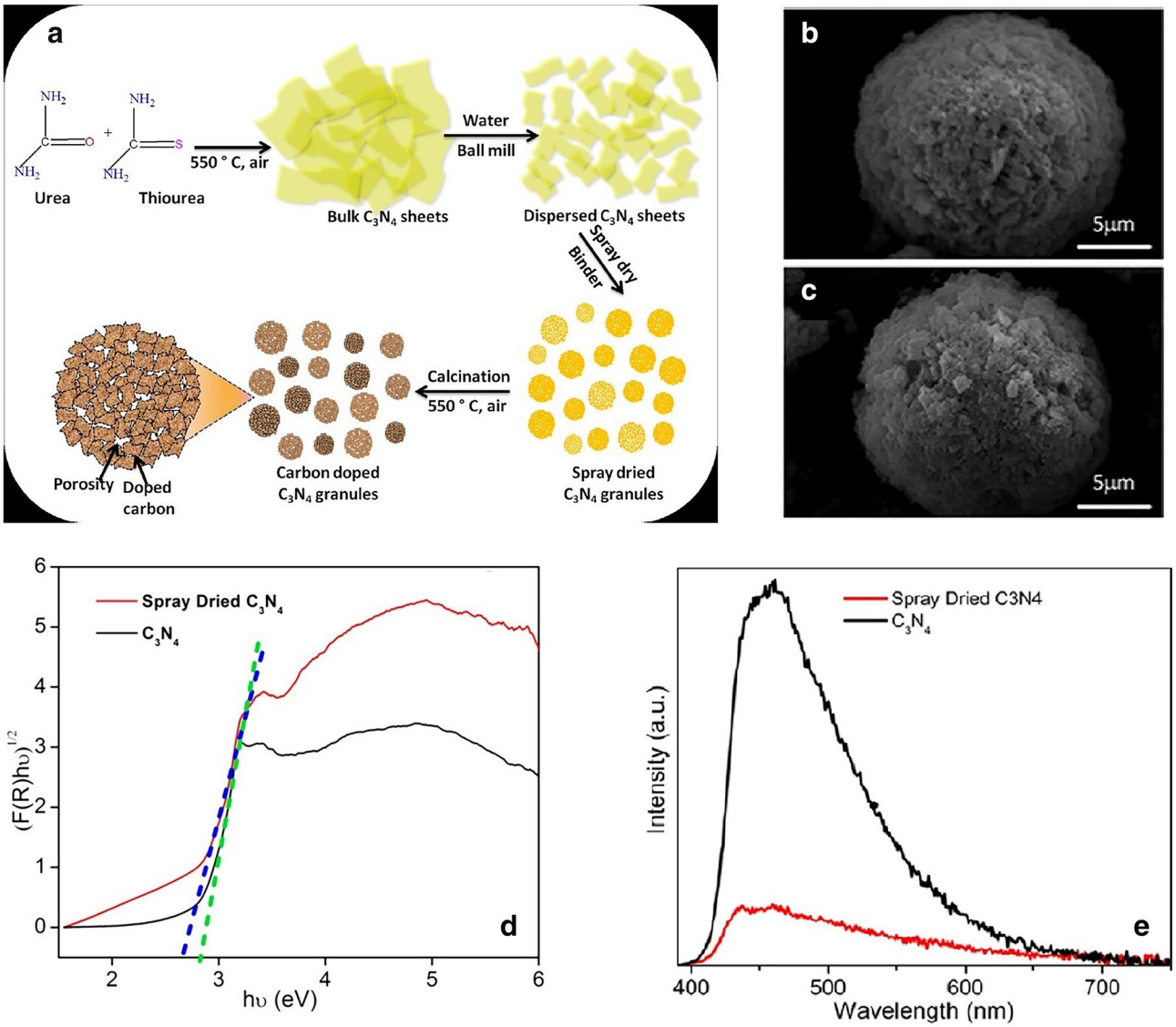

Fig. 3 **a** Synthetic method of spray-dried porous C_3N_4 granules with carbon doping: g-C_3N_4 nanosheets are spray granulated to microspheres, which, after thermal oxidation treatment, resulted in in situ doping of carbon; scanning electron microscope (SEM) images of spray-dried C_3N_4 granules **b** before calcination and **c** after calcination; **d** bandgap estimation from diffuse reflectance spectra (DRS) analysis; **e** photoluminescence (PL) emission spectra show lowered e^-–h^+ recombination for spray-dried C_3N_4 than bulk C_3N_4 (Panneri et al. 2017)

Yu et al. synthesized OV-rich $Bi_2O_2CO_3$ (OV-BOC) by a solution precipitation method which showed greater TCH degradation efficiency than BOC under visible light (Fig. 4a) (Yu et al. 2018). The synthesis method was similar to BOC preparation, but additionally, glyoxal was used in case of OV-BOC, which reduced Bi^{3+} resulting in the evacuation of a few atomic oxygen atoms from the BOC structure. Observations from electron paramagnetic resonance (EPR) spectra validated the presence of OV, with a prominent signal for OV-BOC, as opposed to the BOC spectrum with almost no signal (Fig. 4b). Although $Bi_2O_2CO_3$ is a perovskite, its layered structure aids the separation of e^-–h^+ pairs and it is a wide-bandgap (3.3–3.5 eV) semiconductor. Thus, the introduction of OV in BOC narrows its bandgap (Fig. 4c), making it a visible-light-active photocatalyst with a modified band structure (Fig. 4d). Hailili et al. synthesized OV-rich $CaCu_3Ti_4O_{12}$ photocatalyst for TC degradation (Hailili et al. 2018). The ample OV and defects in the surface of $CaCu_3Ti_4O_{12}$ (i.e., Ti^{3+} and Cu^+) make it visible light active, and they also act as e^- capture sites to increase the e^-–h^+ pair separation, thus boosting its photocatalytic efficiency. There are not many reports of vacancy engineered photocatalysts for pharmaceutical degradation, which leaves scope for further studies. The efficiency of vacancy engineered

Table 2 Efficiency of doped and vacancy engineered photocatalysts and their operating conditions for visible-light-assisted degradation of pharmaceuticals

Doped photocatalyst	Pharmaceutical	Operating conditions	Degradation efficiency/time (min)	Mineralization efficiency/time (min)	k_{app} (min^{-1})	References
B-doped TiO_2	IBP, FLU	IBP, FLU: 20 mg L^{-1} Catalyst: 1 g L^{-1} Visible light pH: 6.5	IBP: 79.4%/240 FLU: 71%/240	IBP: 65%/240 FLU: 60%/240	IBP: 0.01818 FLU: 0.01319	Bilgin Simsek (2017)
Cu-doped TiO_2	PAR	PAR: 50 mg L^{-1} Catalyst: 4 g L^{-1} Visible light pH: 6	100%/180	–	0.0243	Lin and Yang (2013)
Bi^{3+} self-doped $NaBiO_3$	CBZ	CBZ: 4.725 mg L^{-1} Catalyst: 1 g L^{-1} 500 W Xe lamp with 420-nm cutoff filter pH: 6	99.8%/60	78%/120	0.087	Ding et al. (2017)
C-doped g-C_3N_4	TC	TC: 44.4 mg L^{-1} Catalyst: 0.5 g L^{-1} Sunlight	> 90%/90	70%/90	–	Panneri et al. (2017)
N-doped TiO_2	SP	SP: 10 mg L^{-1} Catalyst: 3 g L^{-1} LED light pH: 6	–	100%/90 min	–	Vaiano et al. (2015)
Mn-doped $SrTiO_3$	TC	TC: 10 mg L^{-1} Catalyst: 1 g L^{-1} 250 W Xe lamp with 420-nm cutoff filter	66.7%/60	40.1%/60	0.0166	Wu et al. (2015)
Cr^{3+}-doped $SrTiO_3$	TC	TC: 10 mg L^{-1} Catalyst: 1 g L^{-1} 250 W Xe lamp with 420-nm cutoff filter	68%/60	–	0.01607	Cai et al. (2015)
Fe-doped $SrTiO_3$	TC	TC: 10 mg L^{-1} Catalyst: 1 g L^{-1} 300 W Xe lamp with 420-nm cutoff filter	71.6%/80	42.5%/80	0.197	Li et al. (2014)
Sr-doped β-Bi_2O_3	TC	TC: 20 mg L^{-1} Catalyst: 0.06 g L^{-1} 500 W Xe lamp with 420-nm cutoff filter pH: 9	90%/120	–	0.051	Niu et al. (2013)
C–N–S tri-doped TiO_2	TC	TC: 5 mg L^{-1} Catalyst: 0.5 g L^{-1} 150 W Xe lamp with/without UV filter pH: 7	> 99%/180	> 67%/180	–	Wang et al. (2011a)
C-sensitized and N-doped TiO_2	SNM	SNM: 5 mg L^{-1} Catalyst: 1 g L^{-1} LED light	95%/300	70%/300	0.0109	Wang et al. (2011b)

Vacancy engineered photocatalyst	Pharmaceutical	Operating conditions	Degradation efficiency/time (min)	Mineralization efficiency/time (min)	k_{app} (min^{-1})	References
$Bi_2O_2CO_3$ with OV	TCH	TCH: 10 mg L^{-1} Catalyst: 1 g L^{-1} 500 W Xe lamp with 420-nm cutoff filter	50%/300	–	–	Yu et al. (2018)

Table 2 (continued)

Vacancy engineered photocatalyst	Pharmaceutical	Operating conditions	Degradation efficiency/time (min)	Mineralization efficiency/time (min)	k_{app} (min^{-1})	References
$CaCu_3Ti_4O_{12}$ with OV	TC	TC: 4.45 mg L^{-1} Catalyst: 0.4 g L^{-1} 300 W Xe lamp with 420-nm cutoff filter	99.1%/50	89.58%/50	–	Hailili et al. (2018)

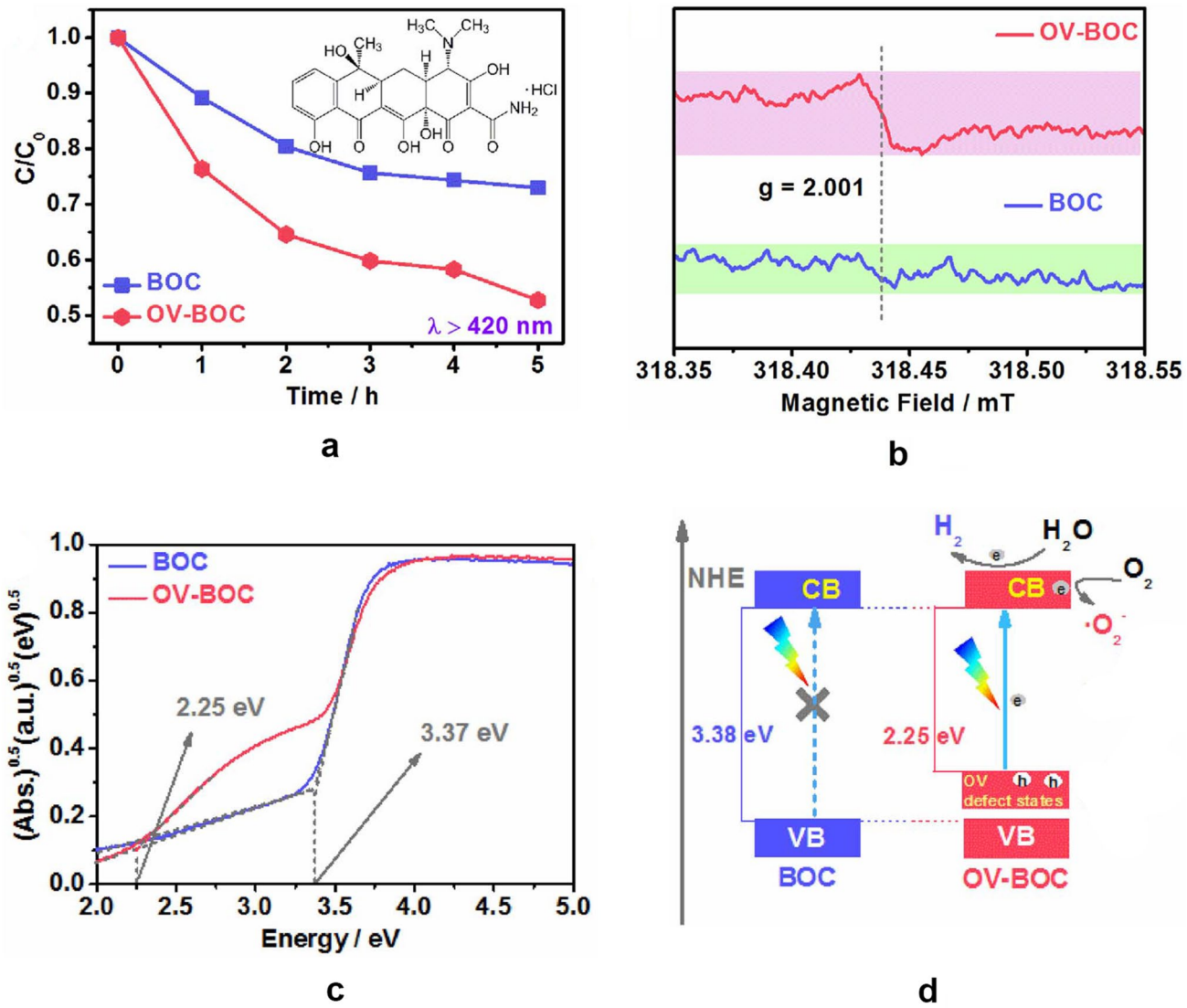

Fig. 4 **a** Photocatalytic degradation of TCH by BOC and OV-BOC, **b** EPR plots, **c** bandgaps, and **d** schematic of band structure of BOC and OV-BOC (Yu et al. 2018)

photocatalysts for visible-light-assisted pharmaceutical degradation along with their detailed reaction conditions is given in Table 2.

Noble metal-deposited semiconductor photocatalysts

The noble metals, for example, Pt, Pd, Au, Ag, and Cu, can be deposited on semiconductors to increase their

photocatalytic efficiency by enhancing the visible light response due to localized surface plasmon resonance and minimizing the e^-–h^+ pair recombination due to Schottky barrier formation (Ray and Pal 2017). However, noble metals (NMs) beyond the optimal loading value will occupy the active sites of photocatalyst resulting in increased e^-–h^+ recombination, lowering the photocatalytic activity (Han et al. 2013; Luo et al. 2015). Localized surface plasmon resonance (LSPR) results in the collective oscillation of the free e^- within the NMs when it absorbs the incident light. The maximum amplitude of oscillation is reached when the frequencies of the incident light and the oscillating free e^- match (Khan et al. 2015). The Schottky barrier formation at the interface of NM–semiconductor mainly relies upon the NM work function (W_M) [i.e., energy difference between the Fermi level (E_F) of NM and the vacuum energy level (V_{ac})] and the semiconductor electron affinity (X_{SM}) (i.e., energy difference between the CB minimum of semiconductor and V_{ac}). In the case of an n-type semiconductor, the W_M is greater than the work function of the semiconductor (W_S), as shown in Fig. 5a. When the NM comes in contact with the semiconductor, the free e^- in the semiconductor migrates to the NMs until equilibrium E_F is reached, which results in upward bending of the band edges, leading to Schottky barrier formation ($\Phi_B = W_M - X_{SM}$) (Fig. 5b). In case of a p-type semiconductor, where the W_M is smaller than the W_S, the free e^- from NM will migrate to the semiconductor (Fig. 5c), resulting in downward bending of band edges (Fig. 5d). The Schottky barrier restricts the backflow of e^- to the semiconductor, making the NM a sink for photogenerated e^- (Khan et al. 2015). The mechanism of visible light photocatalysis of pharmaceuticals by NM-deposited photocatalysts is presented in Fig. 5e.

Ag and Au are both plasmonic metals with excellent charge separation and photo-stability properties. Ag is a popular NM that has been used to enhance the photocatalytic efficiencies of semiconductors such as Bi_3TaO_7 (Luo et al. 2015), $AgIn_5S_8$ (Deng et al. 2018), g-C_3N_4 (Zhang et al. 2016), monodisperse TiO_2 aggregates (Han et al. 2013) and hollow TiO_2 nanoparticles (Boxi and Paria 2015) for visible-light-aided pharmaceutical degradation. The bandgap energy was substantially decreased to 2.25 eV for the Ag-doped hollow TiO_2 as compared to pure TiO_2 ($E_g = 3.2$ eV) (Boxi and Paria 2015). Visible light irradiation leads to the flow of photogenerated e^- from the semiconductor to the Ag where it combines with the LSPR-induced h^+. While

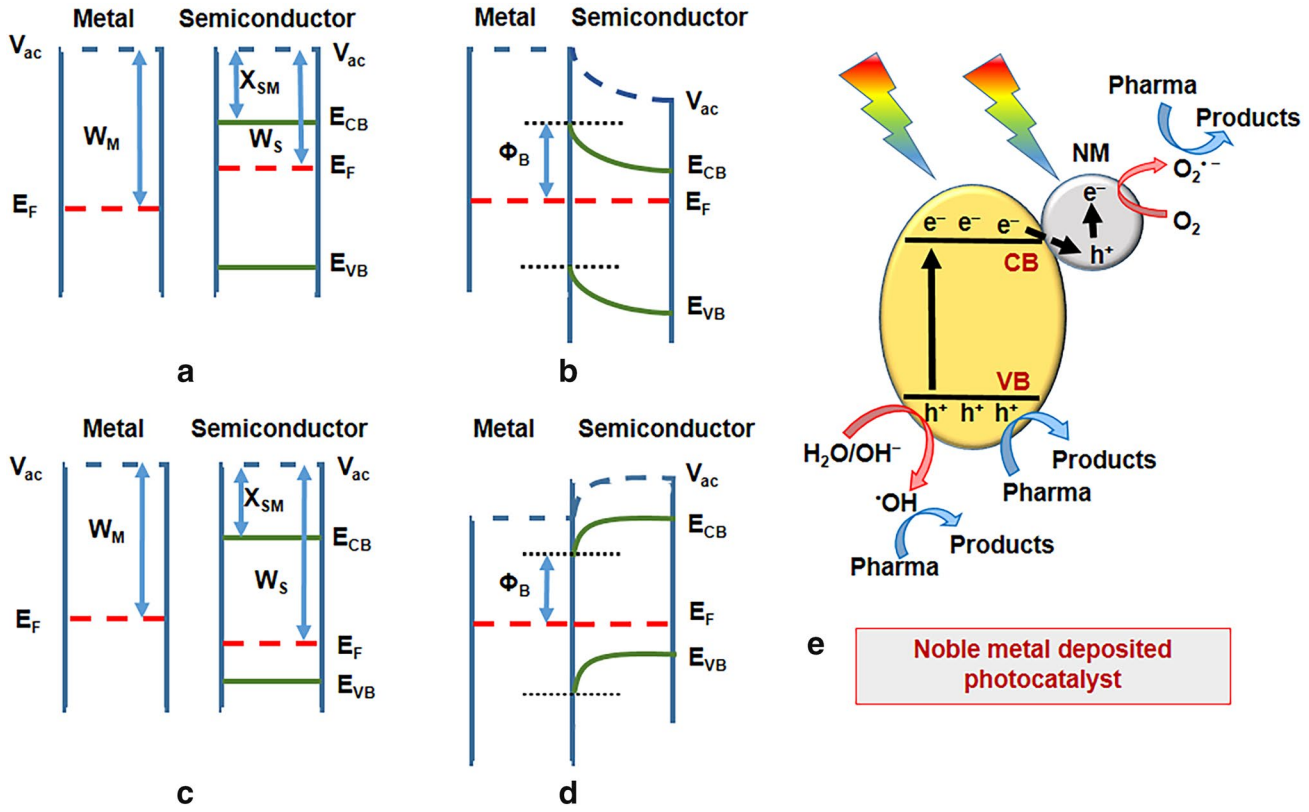

Fig. 5 Formation of the Schottky barrier between n-type semiconductors and NMs **a** before contact and **b** after contact; formation of the Schottky barrier between p-type semiconductors and NMs **c** before contact and **d** after contact; **e** mechanism of pharmaceutical degradation by NM-deposited photocatalyst

the Schottky barrier prevented the e^-–h^+ recombination, the LSPR-induced e^- on the Ag takes part in the reduction of O_2 to $O_2^{\cdot-}$ to improve the photocatalytic performance. Another study reported the Ag-$BiVO_4$ and Cu-$BiVO_4$ photocatalysts for the degradation of IBP (Bian et al. 2014). Jiang et al. developed visible-light-responsive Au/$KCa_2Nb_3O_{10}$ photocatalyst for degradation of TCH (Jiang et al. 2018).

Both Pt and Pd have highly positive work function values that allow them to act as sinks for the photogenerated e^- from the CB of the semiconductors, which consequently inhibits the e^-–h^+ recombination and increases the photocatalytic efficiency (Debnath et al. 2018). WO_3 has a narrow bandgap, but high charge carrier recombination subdues its photocatalytic efficiency. A study reported that WO_3 nanosheets modified with Pt exhibit enhanced photocatalytic activity than WO_3 nanosheets alone for TC degradation (Zhang et al. 2014).

Xue et al. synthesized bimetallic Au and Pt nanoparticles (NPs) co-decorated g-C_3N_4 (Au/Pt/g-C_3N_4) plasmonic photocatalyst that has shown better performance for degrading TCH, as compared to pure g-C_3N_4 and single NM-deposited g-C_3N_4 (Fig. 6a) (Xue et al. 2015a). Visible light irradiation on Au NPs generates free e^- due to LSPR, which flow to the CB of g-C_3N_4, leaving h^+ on Au NPs. As e^- are photogenerated in g-C_3N_4 as well, the excess e^- flow to the Pt NPs as the CB of g-C_3N_4 is more negative than the work function of Pt (Fig. 6b). Coupling the LSPR effect of Au and electron-sink function of Pt NPs with g-C_3N_4 increased the e^-–h^+ pair separation (Fig. 6c) and visible-light-harvesting capacity (Fig. 6d), boosting photocatalysis. The efficiencies of NM-deposited photocatalyst for visible-light-assisted pharmaceutical degradation along with their detailed reaction conditions are given in Table 3.

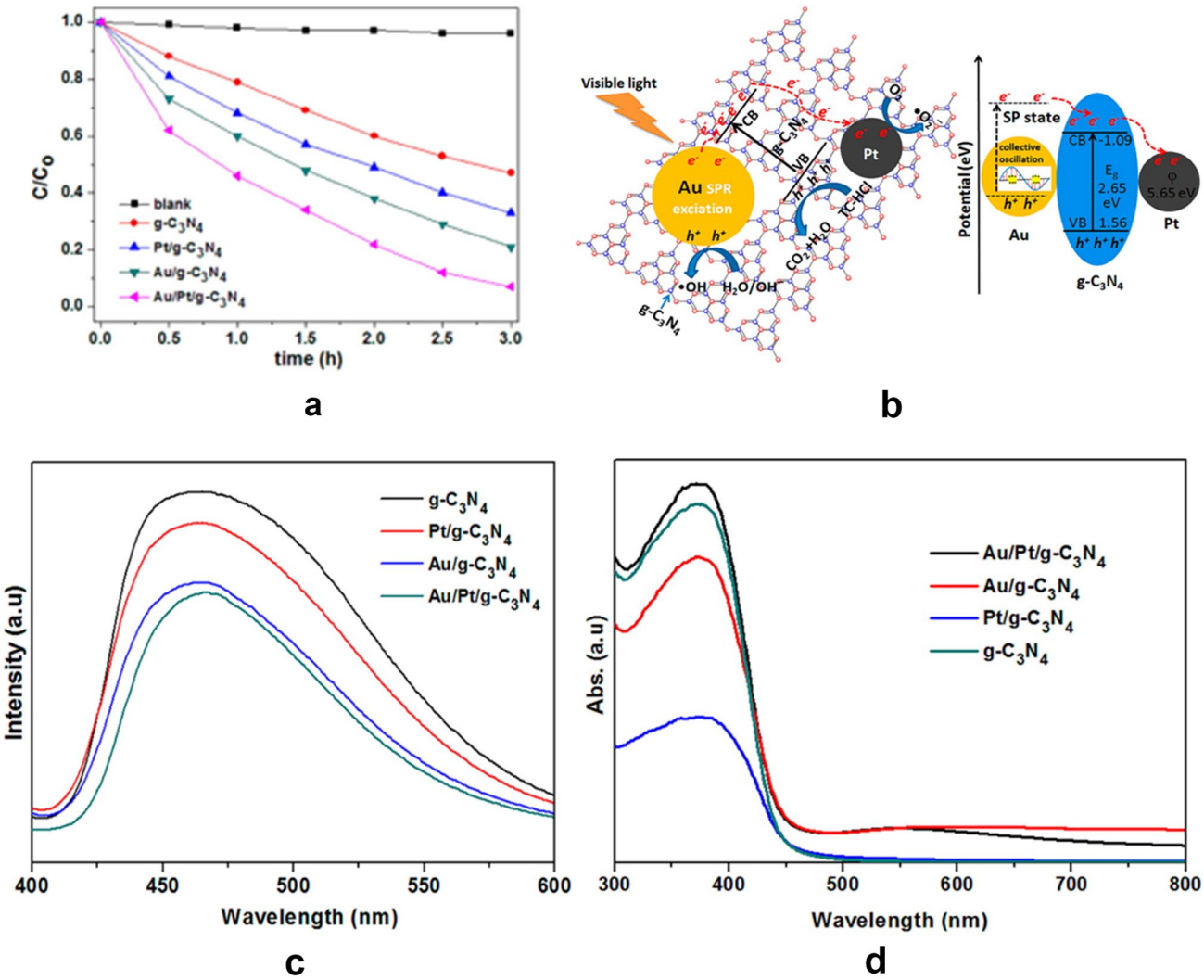

Fig. 6 **a** Photocatalytic activities of g-C_3N_4, Pt/g-C_3N_4, Au/g-C_3N_4, and Au/Pt/g-C_3N_4 for degradation of TCH; **b** degradation mechanism of TCH by Au/Pt/g-C_3N_4; **c** PL emission spectra; and **d** DRS of g-C_3N_4, Pt/g-C_3N_4, Au/g-C_3N_4, and Au/Pt/g-C_3N_4 (Xue et al. 2015a)

Table 3 Efficiency of NM-deposited photocatalysts for visible-light-assisted degradation of pharmaceuticals and their operating conditions

NM-deposited photocatalyst	Pharmaceutical	Operating conditions	Degradation efficiency/time (min)	Mineralization efficiency/time (min)	k_{app} (min^{-1})	References
Ag-doped hollow TiO_2	Metronidazole (MTZ)	MTZ: 30 mg L^{-1} Catalyst: 0.5 g L^{-1} 125 W Hg lamp	94.77%/120	–	0.024	Boxi and Paria (2015)
Ag/g-C_3N_4	DCF	DCF: 100 mg L^{-1} Catalyst: 0.1 g L^{-1} 300 W Xe lamp with UV cutoff filter	100%/120	46.5%/120	0.0429	Zhang et al. (2016)
Au/$KCa_2Nb_3O_{10}$	TCH	TCH: 35 mg L^{-1} Catalyst: 1 g L^{-1} 500 W tungsten lamp	75%/120	–	0.0106	Jiang et al. (2018)
Ag/$AgIn_5S_8$	TCH	TCH: 10 mg L^{-1} Catalyst: 0.4 g L^{-1} 300 W Xe lamp with 400-nm cutoff filter	95.3%/120	83%/240	0.023	Deng et al. (2018)
Ag/Bi_3TaO_7	TC	TC: 10 mg L^{-1} Catalyst: 0.5 g L^{-1} 250 W Xe lamp with 420-nm cutoff filter	85.42%/120	–	0.0162	Luo et al. (2015)
Au/Pt/g-C_3N_4	TCH	TCH: 20 mg L^{-1} Catalyst: 1 g L^{-1} 500 W Xe with 400-nm cutoff filter	93%/180	–	0.4286	Xue et al. (2015a)
Pt/g-C_3N_4	TCH	TCH: 20 mg L^{-1} Catalyst: 1 g L^{-1} 500 W Xe with 400-nm cutoff filter	67.2%/180	–	0.1809	Xue et al. (2015a)
Au/g-C_3N_4	TCH	TCH: 20 mg L^{-1} Catalyst: 1 g L^{-1} 500 W Xe with 400-nm cutoff filter	78.6%/180	–	0.2495	Xue et al. (2015a)
Pt/WO_3 nanosheets	TC	TC: 20 mg L^{-1} Catalyst: 1 g L^{-1} 250 W Xe lamp with 420-nm cutoff filter	72.82%/60	49.66%/60	0.0202	Zhang et al. (2014)
Ag-decorated monodisperse TiO_2	OTC	OTC: 0.5 mg L^{-1} Catalyst: 0.5 g L^{-1} 2 nos. 15 W fluorescent lamps with/without UV filter pH: 5.8	100%/45	–	–	Han et al. (2013)
Cu–$BiVO_4$ Ag–$BiVO_4$	IBP	IBP: 10 mg L^{-1} Catalyst: 0.8 g L^{-1} 300 W Xe lamp with 420-nm cutoff filter	Cu–$BiVO_4$: 89%/300 Ag–$BiVO_4$: 96%/300	–	Cu–$BiVO_4$: 0.008 Ag–$BiVO_4$: 0.011	Bian et al. (2014)

Semiconductor photocatalysts with heterojunctions

Heterojunctions offer the advantages of photogenerated e^-–h^+ pair separation with the combined beneficial effects of the individual semiconductors. Compared to the doping method, heterojunctions have been more suitable for broadening the solar light absorption spectrum (Priya et al. 2016a). The heterojunction configuration as depicted in Fig. 7, where the CB and VB levels of semiconductor1 (S1) are higher than the CB and VB levels of semiconductor2 (S2), is reported in the literature as type II heterojunction (Xu et al. 2018). The charge flow mechanism of Type II heterojunction can be explained with the help of Fig. 7. Type II heterojunction can exist between a p-type and an n-type semiconductor, with the p-type semiconductor having higher band edge levels and work function value than the n-type (Fig. 7c). After contact, the flow of free e^- from n-type to p-type semiconductor takes place until equilibrium E_F is achieved (Fig. 7d), resulting in positively charged n-type and negatively charged p-type semiconductors at the heterojunction interface. Thus, the formation of an internal electric field with the consequent formation of a potential barrier due to band edge bending takes place. With incident light, the internal electric field facilitates the transport of photogenerated e^- from the CB of p-type to the CB of n-type and photogenerated h^+ from the VB of n-type to the VB of p-type (Fig. 7e), which also results in e^-–h^+ pair separation. The heterojunctions can be classified into two types based on the charge carrier flow mechanism: (1) heterojunctions with unidirectional charge flow and (2) heterojunctions with bidirectional charge flow.

Heterojunctions with unidirectional charge flow

In this type of heterojunctions (Fig. 7a), only the S1 is photoactive under the incident light to generate the e^-–h^+ pairs. Therefore, only the photogenerated e^- on the CB of S1 will flow to the CB of S2. As S2 cannot generate the e^-–h^+ pairs under the given lighting condition, there will be no transfer of photogenerated h^+ from the VB of S2 to the VB of S1. Thus, the flow of charge is in one direction. The accumulated e^- on the CB of S2 and h^+ in the VB of S1 will participate in degradation reactions, given that the band edge potentials

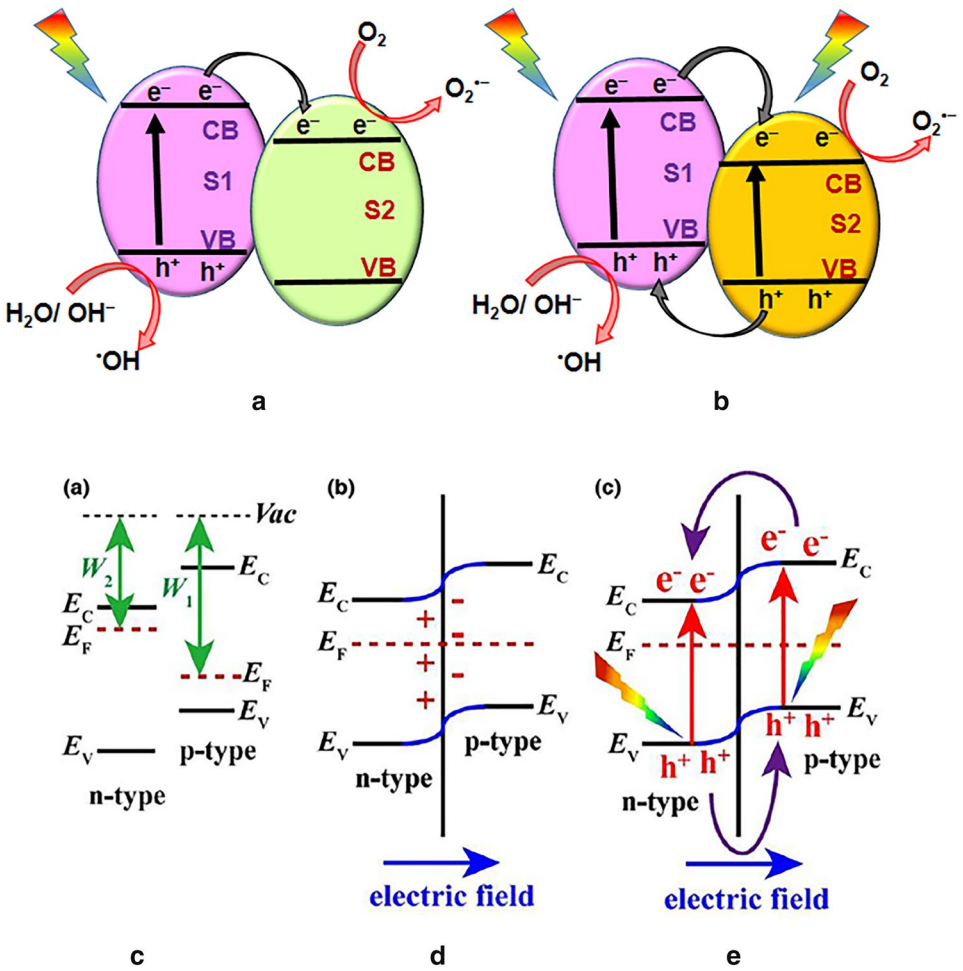

Fig. 7 Schematic of **a** heterojunctions with unidirectional charge flow and **b** heterojunctions with bidirectional charge flow; *schematic of p–n junction: **c** before contact **d** after contact **e** transfer of photogenerated charge carriers in p–n junction mode *(Xu et al. 2018)

of the semiconductors are suitable for the formation of the ROS.

For instance, BiOI is a p-type visible-light-active semiconductor with fast recombination of photogenerated e^-–h^+ pairs, while SnO_2 is an n-type broad bandgap semiconductor with a poor visible light response. Their heterojunction enhanced the photocatalytic efficiency toward OTC degradation due to the increased e^-–h^+ separation, with SnO_2 acting as the sink for photogenerated e^- (Wen et al. 2017). Wang et al. reported a core–shell In_2S_3@MIL-125(Ti) photocatalyst for TC degradation, where stable, visible-light-active In_2S_3 was coupled to an unstable photocatalyst, MIL-125(Ti) with no visible light response (Wang et al. 2016a). Similarly, the degradation efficiency of In_2S_3/Zn_2GeO_4 photocatalyst toward acetaminophen (APAP) due to improved visible light absorption, and greater e^-–h^+ pair separation was reported (Yan et al. 2017b). Graphitic carbon nitride has been used in the formation of heterojunction systems with other semiconductors acting as a sink of the photogenerated charge carriers to enhance the photocatalytic efficiency under visible light irradiation. For example, Jiang et al. constructed a 2D–2D heterostructure with g-C_3N_4 and $K^+Ca_2Nb_3O_{10}^-$ perovskite nanosheets with a wide bandgap of 3.4 eV, for efficient degradation of TCH (Jiang et al. 2017). Interestingly, the 2D–2D heterostructure provides a large contact area for fast interfacial charge separation as well as a broadening the optical window for effective light harvesting as compared to 0D–2D and 1D–2D heterostructures (Cheng et al. 2015).

All the above studies have been performed with visible light which could activate only one of the semiconductors. Thus, it will be imperative to see how such systems, containing both UV and visible-light-active photocatalysts, will respond to solar light. Hong et al. synthesized Nb_2O_5/g-C_3N_4 heterojunction photocatalyst and studied its efficiencies under both visible and solar light toward pharmaceutical

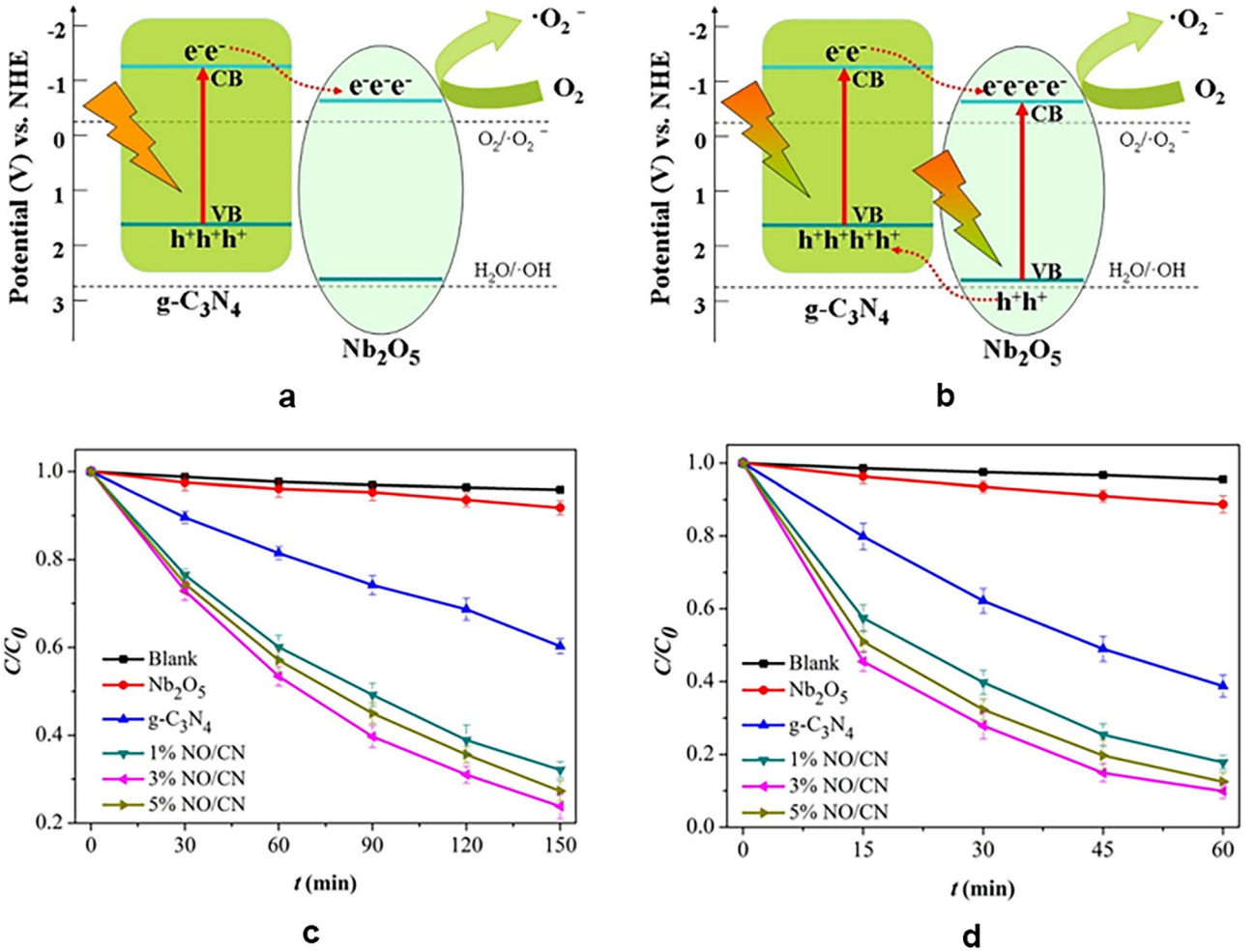

Fig. 8 Schematic of the charge carriers separation and transfer in the Nb_2O_5/g-C_3N_4 heterojunctions under **a** visible and **b** solar light irradiation; photocatalytic efficiency of Nb_2O_5/g-C_3N_4 heterojunctions under **c** visible and **d** simulated solar light irradiation (Hong et al. 2016)

degradation (Hong et al. 2016). He reported the enhanced efficiency of the photocatalyst under solar light due to the photogeneration of e^-–h^+ pairs in both the semiconductors as compared to single photocatalyst excitation under visible light (Fig. 8). Thus, it can be safely asserted that this system has the best output under solar light. A few more examples are found in Sect. 3.5.2 of this review. The efficiency of heterojunctions with unidirectional charge flow for the visible-light-assisted degradation pharmaceuticals along with the detailed reaction conditions is given in Table 4.

Heterojunctions with bidirectional charge flow

In this type of heterojunctions (Fig. 7b), both the semiconductors produce e^-–h^+ pairs under the incident light. Thus, the photogenerated e^- on the CB of S1 will flow to CB of S2, while the photogenerated h^+ on the VB of S2 will flow to VB of S1. Here, the flow of charge is bidirectional. The accumulated e^- and h^+ on the CB and VB of the S2 and S1 actively participate in degradation reactions, provided that the band edge potentials of the semiconductors are suitable for the formation of the ROS.

Some examples of this system using purely visible light have been reported. Ren et al. synthesized a magnetic $NiFe_2O_4/Bi_2O_3$ heterojunction system for photocatalytic degradation of TC, where both the semiconductors have a narrow bandgap, and both are visible light active (Ren et al. 2014). Similarly, g-C_3N_4 has been combined with two narrow bandgap semiconductors $Bi_4O_5Br_2$ (Ji et al. 2017), and Bi_2WO_6 (Wang et al. 2017a) to form heterojunctions, which effectively degrades CIP and IBP, respectively. Shi et al. used CdS QDs/N-doped TiO_2 photocatalyst to effectively mineralize diclofenac (DCF) (Shi et al. 2015).

Examples of this system using solar light irradiation have also been reported. As mentioned earlier, Hong et al. synthesized Nb_2O_5/g-C_3N_4 heterojunction photocatalyst for degradation of TCH, CIP, and levofloxacin (LEV) under simulated solar light irradiation (Hong et al. 2016). Bi_2O_3 has been coupled with wide-bandgap semiconductors such as $(BiO)_2CO_3$ (Chen et al. 2018) and TiO_2 (Sood et al. 2016) to form heterojunctions that have used both the UV and visible spectra of the solar radiation to degrade CIP and OFL, respectively, efficiently. The efficiencies of heterojunctions with bidirectional charge flow for visible-light-assisted pharmaceuticals degradation along with their detailed reaction conditions are compiled in Table 4.

The advantages of heterojunctions in enhancing the charge separation come at the cost of the redox ability of e^- and h^+, which may fall short in concluding a particular photocatalytic reaction (Natarajan et al. 2018). Thus, the composite semiconductor systems with or without redox mediators have been developed to overcome this limitation of heterojunctions (Xu et al. 2018).

Z-scheme photocatalysts

Z-schemes are inspired by the natural photosynthetic process of water splitting (Natarajan et al. 2018). Although the band structure configuration of the Z-scheme photocatalyst is same as that of the heterojunction, the mechanism of charge carrier transfer is different, as depicted in Fig. 9. This exciton transfer mechanism promotes the recombination of photogenerated e^- and h^+ with weaker redox abilities, which spatially separates and preserves the photogenerated e^- and h^+ with superior redox abilities for participating in photocatalytic reactions (Xu et al. 2018). Additionally, the narrow bandgap semiconductors can be selected to build Z-scheme systems to extend the light absorption range, without sacrificing the requisite high redox ability of the photocatalyst. Based on current literature survey focused on visible-light photocatalytic pharmaceutical degradation, the Z-scheme photocatalysts have been classified into two types depending upon the presence of charge carrier mediator: (1) Z-scheme photocatalysts with solid-state electron mediators and (2) Z-scheme photocatalysts without electron mediators or direct Z-scheme photocatalysts.

Z-scheme photocatalysts with solid-state electron mediators

In a Z-scheme photocatalyst with solid-state electron mediators (SSEM), there is a solid electron mediator (Ag, Au, Cu, graphene or carbon, etc.) bridging the two semiconductors through which the charge transfer takes place (Xu et al. 2018). The CB and VB levels of semiconductor1 (S1) are higher than the CB and VB levels of semiconductor2 (S2), and both the semiconductors produce e^-–h^+ pairs under the incident light. Here, the photogenerated e^- on the CB of S2 and the photogenerated h^+ on the VB of S1 will transfer to the SSEM where they will recombine. Meanwhile, the e^- in the CB of S1 and the h^+ in the VB of S2 would become free to participate in degradation reactions, provided that the band edge potentials of the semiconductors are suitable for the formation of the ROS (Fig. 9a). Thus, charge carriers are swiftly separated by the SSEM, resulting in increased photocatalytic efficiency.

Nitrogen-doped graphene quantum dots (NGQDs) are excellent e^- mediators that accelerate the e^- transfer to improve the charge separation efficiency and enhance the photocatalytic degradation activity. Yan et al. prepared NGQDs-$BiVO_4$/g-C_3N_4 for the degradation of TC, OTC, and CIP antibiotics (Yan et al. 2016). Yan et al. reported NGQDs-BiOI/$MnNb_2O_6$ to degrade TC, OTC, CIP, and doxycycline (DOX) (Yan et al. 2017a). Chen et al. reported the photocatalytic degradation of TC by Ag/Ag_3PO_4/$BiVO_4$/reduced graphene oxide (RGO) nanocomposite photocatalyst, where Ag acts as the mediator in separating e^-–h^+ pairs,

Table 4 Efficiency of heterojunctions with unidirectional and bidirectional charge flow for visible-light-assisted pharmaceuticals degradation with the detailed operating conditions

Heterojunction photocatalyst with unidirectional charge flow	Pharmaceutical	Operating conditions	Degradation efficiency/time (min)	Mineralization efficiency/time (min)	k_{app} (min^{-1})	References
g-C_3N_4/$K^+Ca_2Nb_3O_{10}^-$	TCH	TCH: 35 mg L^{-1} Catalyst: 1 g L^{-1} 500 W tungsten lamp	81%/90	–	–	Jiang et al. (2017)
In_2S_3/Zn_2GeO_4	APAP	APAP: 5 mg L^{-1} Catalyst: 1 g L^{-1} Xe lamp with cutoff filter pH: 9	95%/360	55%/360	0.4458	Yan et al. (2017b)
SnO_2/BiOI	OTCH	OTCH: 10 mg L^{-1} Catalyst: 1 g L^{-1} 300 W Xe lamp with 420-nm cutoff filter pH: 5.49	94%/90	–	0.03113	Wen et al. (2017)
In_2S_3@MIL–125(Ti)	TC	TC: 46 mg L^{-1} Catalyst: 0.3 g L^{-1} 500 W Xe lamp with 420-nm cutoff filter	63.3%/60	–	–	Wang et al. (2016a)
Nb_2O_5/g-C_3N_4	TCH	TCH: 20 mg L^{-1} Catalyst: 1 g L^{-1} 250 W Xe lamp with 420-nm cutoff filter	76.2%/150	–	0.0096	Hong et al. (2016)
Heterojunction photocatalyst with bidirectional charge flow	Pharmaceutical	Operating conditions	Degradation efficiency/time (min)	Mineralization efficiency/time (min)	k_{app} (min^{-1})	References
g-C_3N_4/Bi_2WO_6	IBP	IBP: 5.16 mg L^{-1} Catalyst: 0.2 g L^{-1} 300 W Xe lamp with 420-nm cutoff filter	96.1%/60	78.1%/240	0.052	Wang et al. (2017a)
CdS QDs/N-doped TiO_2	DCF	DCF: 50 mg L^{-1} Catalyst: 1 g L^{-1} 1000 W Xe lamp with 420-nm cutoff filter	–	65%/360	–	Shi et al. (2015)
Nb_2O_5/g-C_3N_4	TCH, CIP, LEV	TCH, CIP, LEV: 20 mg L^{-1} Catalyst: 1 g L^{-1} 250 W Xe lamp Solar simulator pH: 3	TCH: 90.2%/60 CIP: > 60%/60 LEV: > 70%/60	TCH: 65.3%/60	TCH: 0.038	Hong et al. (2016)
Bi_2O_3/TiO_2	OFL	OFL: 25 mg L^{-1} Catalyst: 0.5 g L^{-1} Sunlight pH 7	92%/120	–	–	Sood et al. (2016)
g-C_3N_4/$Bi_4O_5Br_2$	CIP	CIP: 10 mg L^{-1} Catalyst: 0.5 g L^{-1} 300 W Xe lamp with 400-nm cutoff filter Solar simulator	50%/30	–	–	Ji et al. (2017)
Bi_2O_3/$(BiO)_2CO_3$	CIP	CIP: 10 mg L^{-1} Catalyst: 0.5 g L^{-1} 300 W Xenon lamp Solar simulator pH: 4.0–8.3	90%/150	20%/150	–	Chen et al. (2018)
$NiFe_2O_4$/Bi_2O_3	TC	TC: 10 mg L^{-1} Catalyst: 1 g L^{-1} 150 W Xe lamp with 420-nm cutoff filter	90.78%/90	51.95%/90	0.36	Ren et al. (2014)

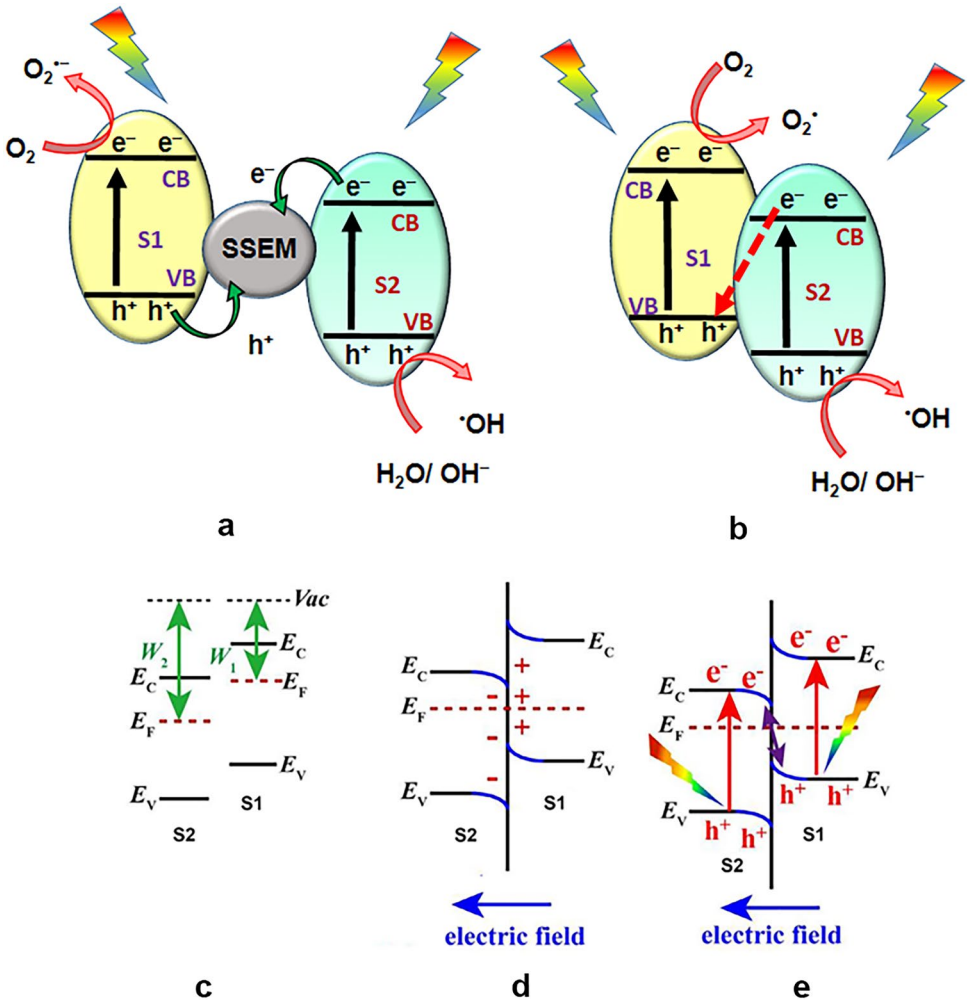

Fig. 9 Schematic representation of **a** Z-scheme photocatalyst with solid-state electron mediators and **b** direct Z-scheme photocatalyst; *schematic representation of direct Z-scheme: **c** before contact, **d** after contact, **e** photogenerated charge carrier transfer process*(Xu et al. 2018)

while RGO adsorbs more TC due to its large surface area and also acts as e^- trapping and transporting site (Chen et al. 2017). Zhu et al. developed polypyrrole (PPy)@Ag/g-C_3N_4 nanocomposite to degrade TC, CIP, gatifloxacin (GFLX), enrofloxacin hydrochloride (EH), and danofloxacin mesylate (DM) with visible light (Zhu et al. 2016). PPy is a narrow bandgap organic semiconductor which can also serve as a protective layer to the Ag nanoparticles exposed to harsh experimental conditions. Ag nanoparticles mediate the photogenerated electron transfer to facilitate efficient e^-–h^+ pair separation. The efficiency of Z-scheme photocatalysts with SSEM for visible-light-assisted pharmaceuticals degradation with their detailed reaction conditions is given in Table 5.

The limitations of this system are the expensive NMs and the difficult synthetic procedures of nanocarbon and graphene, which serve as SSEMs. Another major drawback is the shielding effect, i.e., the blocking of visible light by the metallic SSEMs from reaching the catalyst surface (Natarajan et al. 2018). The feasible solution to such problems was the development of Z-scheme photocatalysts without redox mediators.

Direct Z-scheme photocatalysts

A direct Z-scheme photocatalyst is a combination of two semiconductors (S1 and S2) without electron mediator between them (Fig. 9b). The band edges are higher while work function value is less in S1 as compared to S2 (Fig. 9c). After contact, the flow of free e^- from S1 to S2 takes place until equilibrium E_F is achieved (Fig. 9d). This results in positively charged S1 and negatively charged S2 at the interface. Thus, the formation of an internal electric field with the consequent formation of a potential barrier due to band edge bending takes place. Both the semiconductors produce e^-–h^+ pairs under the incident light. Facilitated by the internal electric field, the photogenerated e^- from the CB of S2 will recombine with the photogenerated h^+ from the VB of S1 (Fig. 9e) promoting spatial separation of e^- and h^+ in the CB of S1 and VB of S2, respectively, which can partake in the redox photocatalytic reactions. Thus, the problem of photon capturing and light shielding by the mediators is abolished by this type of e^-–h^+ pair transfer phenomenon, resulting in greater visible light uptake by the photocatalysts.

Table 5 Efficiency of Z-scheme with SSEM and direct Z-scheme photocatalysts for visible-light-assisted pharmaceuticals degradation with their detailed operating conditions

Z-scheme photocatalyst with SSEM	Pharmaceutical	Operating conditions	Degradation efficiency/time (min)	Mineralization efficiency/time (min)	k_{app} (min^{-1})	Reference
$Ag/Ag_3PO_4/BiVO_4$/RGO	TC	TC: 10 mg L^{-1} Catalyst: 0.5 g L^{-1} 300 W Xe lamp with 420-nm cutoff filter	94.96%/60	27.42%/60	–	Chen et al. (2017)
NGQDs—$BiVO_4$/g-C_3N_4	TC, OTC, CIP	TC, OTC, CIP: 10 mg L^{-1} Catalyst: 0.5 g L^{-1} 250 W Xe lamp with 420-nm cutoff filter	TC: 91.5%/30 OTC: 66.7%/120 CIP: 72.4%/120	TC: 68.9%/30	TC: 0.0804	Yan et al. (2016)
NGQDs—BiOI/$MnNb_2O_6$	TC, OTC, DOX, CIP	TC, OTC, DOX, CIP: 10 mg L^{-1} Catalyst: 0.5 g L^{-1} 250 W Xe lamp with 420-nm cutoff filter	TC: 87.2%/60 OTC: 72.1%/120 DOX: 64.7%/120 CIP: 57.4%/120	–	TC: 0.0331	Yan et al. (2017a)
Ppy @Ag/g-C_3N_4	TC, CIP, GFLX, EH, DM	TC, CIP, GFLX, EH, DM: 10 mg L^{-1} Catalyst: 1 g L^{-1} 300 W Xe	TC: > 90%/60 CIP: > 90%/60 GFLX: > 80%/60 EH: > 90%/60 DM: > 80%/60	–	–	Zhu et al. (2016)
Direct Z-scheme photocatalyst	**Pharmaceutical**	**Operating conditions**	**Degradation efficiency/time (min)**	**Mineralization efficiency/time (min)**	**k_{app} (min^{-1})**	**Reference**
$WO_3/K^+Ca_2Nb_3O_{10}^-$	TCH	TCH: 35 mg L^{-1} Catalyst: 1 g L^{-1} 250 W Xe lamp Solar simulator	85.8%/120	–	0.0151	Ma et al. (2017)
β-Bi_2O_3 @ g-C_3N_4	TC	TC: 10 mg L^{-1} Catalyst: 0.5 g L^{-1} 250 W Xe lamp with 420-nm cutoff filter	80.2%/50	59.2%/50	0.0311	Hong et al. (2018)
AgI/WO_3	TC	TC: 35 mg L^{-1} Catalyst: 1 g L^{-1} 300 W Xe lamp with 420-nm cutoff filter	75%/60	–	0.0235	Wang et al. (2016b)
Bi_3TaO_7 quantum dots/g-C_3N_4	CIP, CPX	CIP, CPX: 10 mg L^{-1} Catalyst: 0.5 g L^{-1} 86 W LED lamp	CIP: 91%/120 CPX: 77%/240	–	CIP: 1.1902 CPX: 0.3728	Wang et al. (2017b)

Additionally, direct Z-scheme photocatalysts are corrosion resistant (Xu et al. 2018).

WO_3 is a stable, economic, eco-friendly narrow band-gap semiconductor (2.4–2.8 eV), having rapid e^-–h^+ pair recombination. Moreover, WO_3 cannot form $O_2^{\cdot-}$ radicals under light irradiation as the CB potential (0.87 eV) is more positive than the $O_2/O_2^{\cdot-}$ potential (–0.046 eV). Wang et al. reported the formation of AgI/WO_3 direct Z-scheme photocatalyst, which suppressed the e^-–h^+ pair recombination and resulted in the efficient visible light TC degradation (Wang et al. 2016b). Both semiconductors are visible light active, resulting in the recombination of the weak photogenerated e^- and h^+ from the CB of WO_3 and VB of AgI, respectively, leaving the strong h^+ and e^- in the VB of WO_3 and CB of AgI, respectively, to take part in the photocatalytic reactions (Fig. 10). Similarly, the photocatalytic performance of $WO_3/K^+Ca_2Nb_3O_{10}^-$ was reported by Ma et al. for TCH degradation under simulated sunlight (Ma et al. 2017).

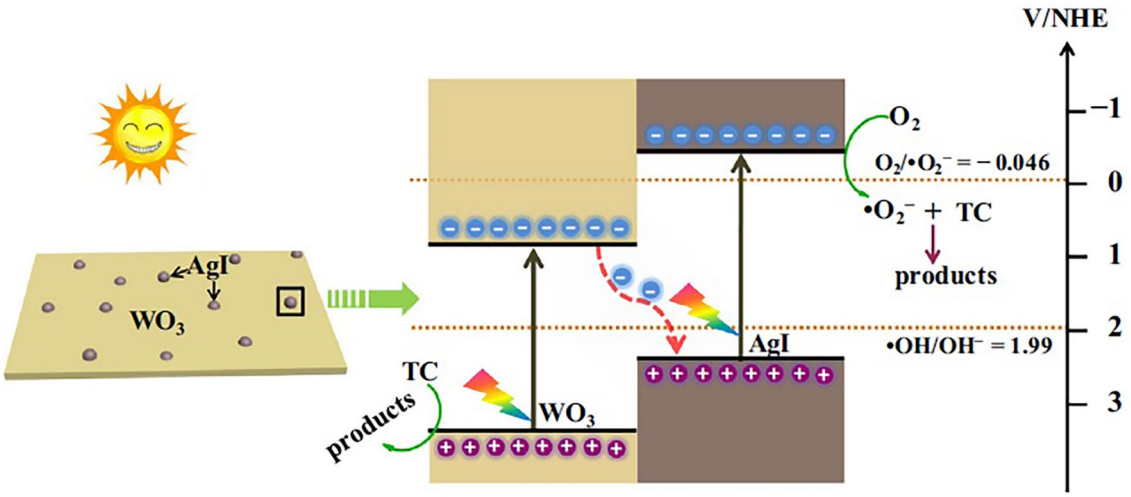

Fig. 10 Mechanism for the photocatalytic degradation of TC on AgI/WO_3 (Wang et al. 2016b)

Studies have reported the use of g-C_3N_4 for the development of β-Bi_2O_3@g-C_3N_4 core/shell (Hong et al. 2018) and Bi_3TaO_7 quantum dots/g-C_3N_4 (Wang et al. 2017b) direct Z-scheme photocatalysts for efficient charge separation and improved visible-light-induced degradation of TC, CIP, and cephalexin (CPX). The efficiency of direct Z-scheme photocatalysts for visible-light-assisted pharmaceuticals degradation with their detailed reaction conditions is given in Table 5.

Other photocatalysts

There are a few interesting photocatalysts that do not fall under the categories of visible-light-active photocatalysts previously mentioned in this review. However, the reaction mechanism of a few of these photocatalysts can be understood from the knowledge of the preceding categories of modified photocatalysts. For example, Chen et al. fabricated an Au and CuS nanoparticles decorated TiO_2 nanobelts (Au–CuS–TiO_2 NBs) photocatalyst for OTC degradation. CuS is an n-type narrow bandgap semiconductor. A p-n heterojunction photocatalyst with enhanced light absorption range is formed by combining TiO_2 and CuS. The addition of Au NPs exhibits LSPR effect that further extends the light-harvesting ability and also increases the e^-–h^+ pair separation on the photocatalyst. The incident solar light induces photogenerated e^-–h^+ pairs in the photocatalyst, resulting in the charge carrier transfer pathway depicted in Fig. 11a (Chen et al. 2016). Photocatalysts such as Ag–AgBr/TiO_2 and Ag-Ag_2O/reduced TiO_2, with similar charge carrier transfer mechanism, were reported in other studies (Wang et al. 2012; Cui et al. 2017).

Liu et al. synthesized $SrTiO_3$ (STO)/Fe_2O_3 nanowires photocatalysts for TC degradation (Liu et al. 2016a). The STO/Fe_2O_3 photocatalyst experiences a phenomenon known as the interfacial charge transfer (IFCT) mechanism. This mechanism extends the light-harvesting range of the photocatalyst by facilitating the migration of photogenerated e^- from the VB of the STO to Fe_2O_3, which partially reduces the Fe^{3+} to Fe^{2+}. The Fe^{2+} reduces O_2 adsorbed on the catalyst surface generating H_2O_2. The photogenerated h^+ in the VB of STO partakes in the photocatalytic reactions. The IFCT spatially separates the charges and inhibits the e^-–h^+ recombination.

Combining photocatalysts with magnetic materials facilitate easy separation after wastewater treatment, prevent catalyst agglomeration, and increase catalyst durability (You et al. 2017). Liu et al. synthesized magnetic zeolite X-supported Ag/AgCl photocatalyst for degradation of TC (Liu et al. 2016b). Magnetic zeolite X facilitated easy catalyst separation, prevented metal leaching, and increased the efficiency of the photocatalyst by reducing the e^-–h^+ recombination (Fig. 11b). Besides, zeolites have been considered as ideal supports due to their properties of ion-exchange, high porosity, and adsorption capacity (Azimi and Nezamzadeh-Ejhieh 2015). A study reported the use of superparamagnetic Bi_2O_4/Fe_3O_4 for IBP degradation (Xia and Lo 2016). In addition to the superparamagnetic properties, Fe_3O_4 acts as a sink of the photogenerated e^- from Bi_2O_4, due to their high conductivity, to reduce the e^-–h^+ recombination. Kumar et al. prepared a magnetic BiOCl/g-C_3N_4/Cu_2O/Fe_3O_4 quaternary heterojunction photocatalyst for both visible-light- and sunlight-assisted degradation of SME (Kumar et al. 2018). A magnetic Fe_3O_4@Bi_2O_3–RGO heterostructured photocatalyst has been developed by Zhu et al. for CIP degradation (Zhu et al. 2017b). Spinel ferrites (AFe_2O_4, A = Mg, Co, Ni or Zn) are narrow bandgap semiconductors having a good magnetic property, chemical stability, but have poor

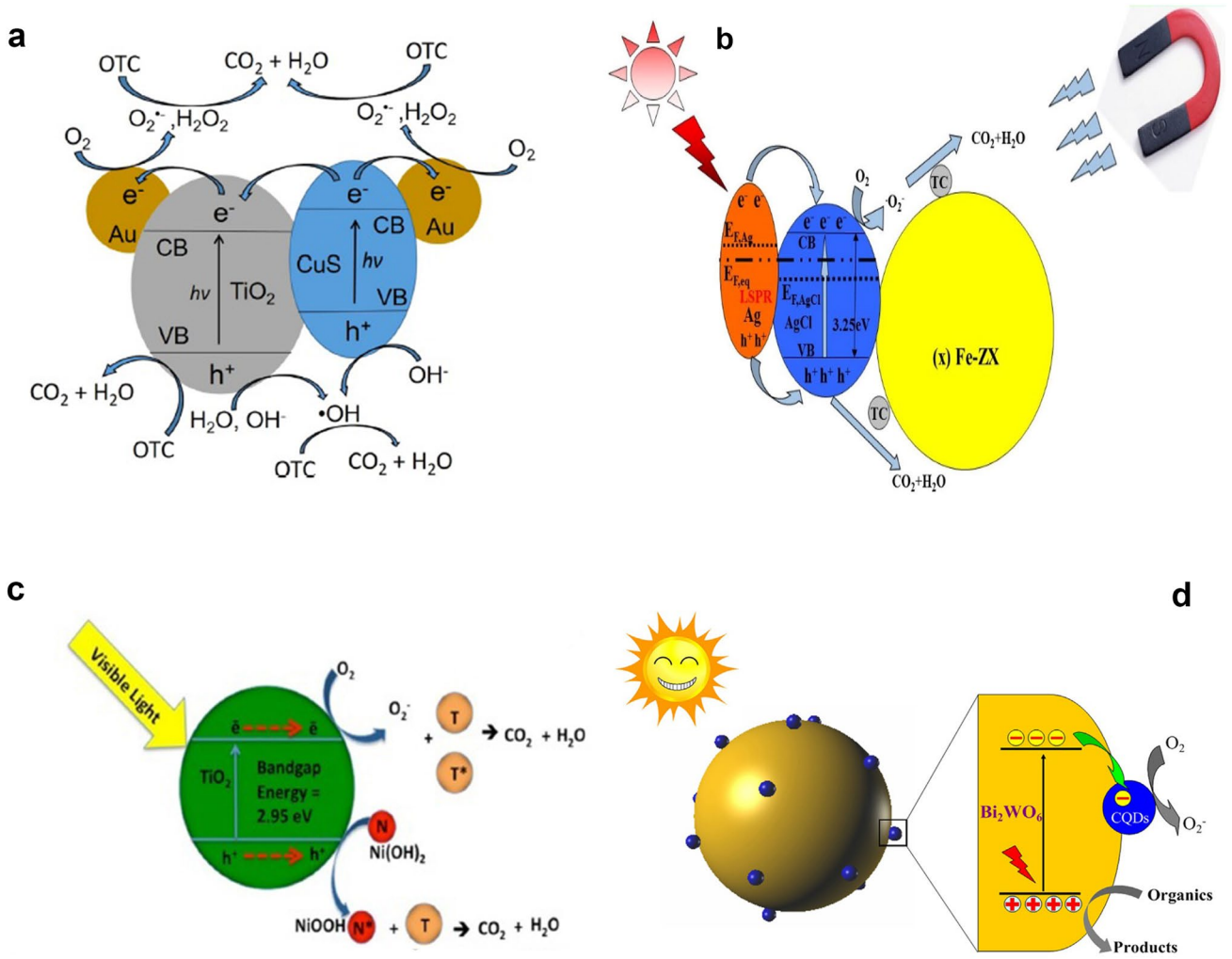

Fig. 11 Proposed visible light photocatalytic degradation mechanism for **a** Au–CuS–TiO_2 NBs system (Chen et al. 2016), **b** magnetic zeolite X-supported Ag/AgCl (Liu et al. 2016b), **c** T1-Ni and T2-Ni (Leong et al. 2016), **d** CQDs/Bi_2WO_6 (Di et al. 2015)

quantum yield due to the low separation of photogenerated e^-–h^+ pairs. To improve e^-–h^+ separation, Hong et al. have doped $NiFe_2O_4$ with copper, to produce a $Ni_{(1-x)}Cu_{(x)}Fe_2O_4$ photocatalyst to degrade TC (Hong et al. 2015).

A study reported the degradation of TC present in wastewater by $Ni(OH)_2$–rutile TiO_2 photocatalyst (Leong et al. 2016). Rutile TiO_2 has a smaller E_g, the faster recombination rate of photoelectron and holes, higher light scattering efficiency, better chemical stability, and lower production cost than anatase TiO_2. Combining $Ni(OH)_2$ with TiO_2 narrows the E_g of $Ni(OH)_2$–TiO_2 making it visible light active and simultaneously reduces the e^-–h^+ recombination. Upon irradiation, the photogenerated h^+ on the VB of TiO_2 oxidizes $Ni(OH)_2$ to NiOOH, which is responsible for oxidizing TC (Fig. 11c). Di et al. synthesized CQDs/Bi_2WO_6 photocatalyst to degrade TC and CIP (Di et al. 2015). Photoinduced e^- on the CB of Bi_2WO_6 migrates to CQDs due to their delocalized conjugated structure promoting efficient charge carrier separation (Fig. 11d). Another study showed the efficient degradation and mineralization of IBP by GQD/$AgVO_3$ photocatalyst (Lei et al. 2016). The efficiency of other photocatalysts for visible-light-assisted pharmaceuticals degradation with their detailed reaction conditions is presented in Table S2.

Photocatalysts with supports

Reusability or recyclability of a photocatalyst is another important factor to be considered for its large-scale use. While the larger particles can be separated by sedimentation or filtration, the small nanoparticles are difficult to separate by economic processes. There is also the requirement of initial adsorption of the pollutant on the photocatalyst surface for efficient photocatalytic degradation. Nano-sized photocatalysts have been immobilized on suitable support materials to solve these problems. Desirable support material

must preferably have excellent adsorbing capacity toward pollutants, endurance, and stability against harsh operating conditions during real field applications, acting as a pool of e^- to minimize e^-–h^+ recombination and facilitate easy separation after intended use.

Naturally abundant materials, for instance diatomite, bentonite, chitosan, etc., have been used as supports for photocatalysts. Chen and Liu developed N-doped TiO_2/diatomite integrated photocatalytic pellet (N-IPP) for degrading TC solution (Chen and Liu 2016). N-doping narrows the E_g of TiO_2 nanoparticles and makes it visible light active, while immobilization on diatomite makes separation after photocatalysis easy (Fig. 12). Another use of diatomite is adsorption of TC due to its high porosity and large surface area. The adsorption of pollutants within its interlayer space makes bentonite (BT) good support for photocatalysts. Gautam et al. reported two spinel ferrites $NiFe_2O_4$ and $MnFe_2O_4$ supported on bentonite, viz. $NiFe_2O_4$/BT and $MnFe_2O_4$/BT, respectively, for the degradation and mineralization of ampicillin (AMP) and OTC antibiotics under solar light (Gautam et al. 2016, 2017). Zuo et al. developed an attapulgite (ATP)/Cu_2O/Cu/g-C_3N_4 composite photocatalyst for chloramphenicol (CAP) degradation (Zuo et al. 2017). Chitosan (CT) is a good bio-adsorbent which is non-toxic and naturally abundant, making it a great choice as a support material. Bi_2O_3/BiOCl/CT and BiOCl/CT have been reported for degradation and mineralization of OTC and AMP under solar light

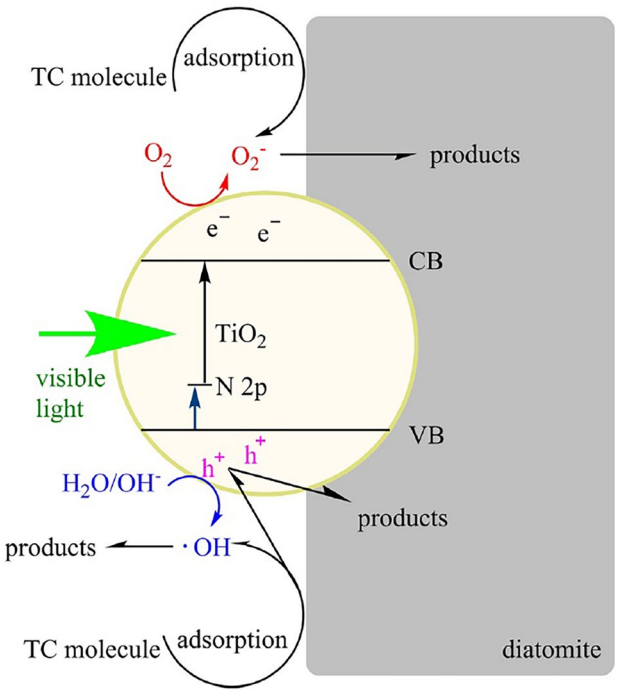

Fig. 12 Schematic illustrating the synergistic effect of photodegradation process of TC using N-IPP (Chen and Liu 2016)

(Priya et al. 2016a, b). Shi et al. synthesized palygorskite-supported Cu_2O–TiO_2 heterojunction composite for TC degradation under solar light (Shi et al. 2016). The heterojunction photocatalyst gave a higher photocatalytic performance under visible light than the individual semiconductors due to a decrease in E_g and increase in e^-–h^+ pair separation. However, the agglomeration of photocatalysts in water was reduced by providing support, palygorskite, an economical, stable, non-toxic, and nonmetallic mineral. Zr-doped TiO_2 nanoparticles immobilized on delaminated clay materials proved to effective photocatalyst for the solar-light-aided degradation of antipyrine (Belver et al. 2017).

Carbonaceous materials are considered as good supports for photocatalysts due to their large surface area and high porosity resulting in high adsorption capacity, and superior electrical conductivity and electron trapping ability for minimizing the e^-–h^+ pair recombination in photocatalysts (Cao et al. 2013; Priya et al. 2016a). Bi_2O_3/BiOCl/graphene sand composite (GSC) and BiOCl/GSC have been reported for degradation and mineralization of OTC and AMP under solar light (Priya et al. 2016a, b). Similarly, GSC-supported $NiFe_2O_4$ ($NiFe_2O_4$/GSC) and $MnFe_2O_4$ ($MnFe_2O_4$/GSC) have been reported for the degradation and mineralization of AMP and OTC antibiotics under solar light (Gautam et al. 2016, 2017). Graphene oxide (GO) was used as a support material to develop Ce-doped TiO_2/GO magnetic composite (Cao et al. 2016), $Ce(MoO_4)_2$ nanocubes/GO composite (Karthik et al. 2017), and Ag_2MoO_4/Ag/AgBr/GO photocatalysts (Bai et al. 2016) for the degradation of pharmaceuticals. GO sheets inhibited the photo-corrosion by trapping electrons and also offered more active sites due to its large surface area to enhance the photocatalysis. RGO has a large surface area to adsorb more pollutants, and it acts as an e^- reservoir due to its high conductivity. CdS suffers from high recombination of e^-–h^+ pairs and instability due to highly oxidation-prone sulfide ion causing photo-corrosion. Tang et al. developed an RGO–CdS/ZnS heterojunction photocatalysts to reduce e^-–h^+ recombination and photo-corrosion of CdS for efficient photocatalytic degradation of TC (Tang et al. 2015). Another study reported the use of RGO–WO_3 composites to degrade sulfamethoxazole (SMX) (Zhu et al. 2017a).

Among emerging support materials, side-glowing optical fibers (SOFs) are great photocatalyst supports as they allow light to pass uniformly along the length of the fiber providing better exposure to the photocatalysts than other supports (Lin et al. 2017a). Lin et al. performed the photocatalytic degradation of IBP, CBZ, and SMX by TiO_2–Fe immobilized on side-glowing optical fibers (Lin et al. 2017a). Doping of TiO_2 with Fe^{3+} narrowed its E_g, making it visible light responsive and also inhibited the

e^-–h^+ recombination, resulting in higher photocatalytic performance. Another study reported the degradation of IBP with TiO_2–RGO immobilized onto SOF (Lin et al. 2017b). The efficiency of photocatalysts with supports for visible-light-assisted pharmaceuticals degradation with their detailed reaction conditions is given in Table S3.

Influence of key parameters on pharmaceutical removal

Light

The formation of photogenerated charge carriers is directly proportional to the intensity of light. As intensity increases, the photocatalyst is exposed to more photons to produce more e^-–h^+ pairs that result in increased reaction rates. Studies reported the increased degradation rate of pharmaceuticals by increasing the light intensity (Belver et al. 2017). Light intensity also varies with the distance between the light source and the point of measurement. As the distance increases, the intensity decreases. Belver et al. also reported that the highest photonic efficiency of the catalyst was obtained at an intensity less than the intensity that resulted in the highest reaction rate (Belver et al. 2017). This implies that increasing the light intensity does not necessarily increase the separation of the e^-–h^+ pairs. The wavelength of light is also an important factor which can affect the rate of degradation. Wang et al. used four different light-emitting diode (LED) strips with the same intensity, emitting white (W), blue (B), green (G), and yellow lights (Y) with main emission wavelengths of 450 nm, 465 nm, 523 nm, and 589 nm, respectively. The SNM degradation and mineralization efficacies with the different irradiations were in the order W > B > G > Y (Wang et al. 2011b).

Solution pH

The prerequisite of photocatalytic degradation is the contact of the pollutant to the photocatalyst surface. Pollutant adsorbed on the surface of the photocatalyst is degraded quicker than in bulk solution. This is due to the obliteration of short-lived charge carriers caused by migration or diffusion. More adsorption ensures greater degradation of pollutants. Thus, the pH of the solution, pKa value of the pollutant and zero-point charge (ZPC) of the photocatalyst are important parameters that dictate the extent of the surface contact or adsorption due to electrostatic interaction. For any photocatalyst, the surface is positively charged at a solution pH lower than the ZPC and negatively charged at a pH higher than ZPC (Mahamallik et al. 2015). The pharmaceutical compounds also show different speciation at different solution pHs depending upon its pKa values. For example, TC has three pKa values of 3.30, 7.68 and 9.68 by virtue of which it is completely protonated (H_3L^+) at pH values < 3.3, the zwitterionic form ($H_2L^{\pm}$) exists at pH 3.3 to 7.68, and two anionic forms HL^- and L^{-2} appear at pH > 7.68 and pH > 9.68, respectively (Mahamallik et al. 2015). Similarly, SMX has two pKa values of 1.8 and 5.6, i.e., the cationic form (SMX^+) prevails at pH ≤ 1.7, and the anionic form (SMX^-) dominates at pH ≥ 5.7, while it is neutral in pH range 1.8–5.6 (Kumar et al. 2018). Thus, favorable condition for electrostatic attraction is a solution pH which will result in unlike charges of the photocatalyst and the pollutant.

Holes can produce $^{\cdot}OH$ from water at any pH, as shown in Eq. (2). While the formation of $^{\cdot}OH$ in acidic condition requires the presence of dissolved oxygen (Eqs. 4–7) and Eqs. (4), (5), (10)–(12), it is not the case in alkaline condition (Eq. 13) (Wang et al. 2011b; Deng et al. 2018).

$$^{\cdot}HO_2 + e^- \rightarrow HO_2^- \tag{10}$$

$$HO_2^- + H^+ \leftrightarrow H_2O_2 \tag{11}$$

$$H_2O_2 + O_2^{\cdot-} \rightarrow {}^{\cdot}OH + OH^- + O_2 \tag{12}$$

$$OH^- + h^+ \leftrightarrow {}^{\cdot}OH \tag{13}$$

However, extreme pH will result in the likeness of charges causing repulsion between the photocatalyst and the pollutant, and the strong alkaline condition will generate an excess of $^{\cdot}OH$ which may block the active site on photocatalysts surface, while the highly acidic medium may cause leaching of some photocatalyst.

Photocatalyst dosage

The photocatalyst dosage plays an important role in the photocatalytic degradation of pharmaceuticals. Increasing the quantity of catalyst increases the surface area, providing added active sites, which boosts the adsorption efficiency to improve the photocatalysis. But it has been found that after a certain dosage, the increase in the quantity of photocatalyst in the solution does not increase the photocatalytic efficiency. The solution becomes turbid due to the huge catalyst load, which inhibits the penetration of light, causing the exposure of light only to a small fraction of the catalyst that is adjacent to the reactor wall. It has also been observed that higher dosage causes agglomeration and sedimentation of the photocatalyst, leading to lower surface area (Wang et al. 2011b). During the photocatalytic degradation of SMX, Kumar et al. reported that k_{app} increases for an increase in the photocatalyst dosage up to 400 mg L^{-1}, after which the k_{app} decreases (Kumar et al. 2018). Hence, optimization of the photocatalyst dosage is vital to produce

maximum efficiency while minimizing the cost. Optimum photocatalyst dosage will vary with the type of pollutant to be degraded.

Initial concentration of pharmaceuticals

When the initial concentration of the pollutant is high, the contest for photon absorption with the photocatalyst increases, causing lesser photons to reach the photocatalyst surface. Thus, the photocatalytic efficiency deteriorates with the increase in the initial concentration of the pollutant. Chen et al. found that higher initial concentration of CIP caused lesser photocatalytic degradation (Chen et al. 2018). Wang et al. have reported a similar observation during SNM degradation, where they also predicted that the end products and intermediates of photodegradation might compete with the parent organic molecules for the absorptive and reactive sites on the photocatalyst surface, to hinder the photocatalytic efficiency (Wang et al. 2011b).

Reaction time

The intermediates and by-products formed during the photocatalysis of the pharmaceuticals may be toxic, sometimes even more than the parent compound. Hence, proper evaluation of the reaction time is required to ensure either complete mineralization or enough mineralization to produce harmless products. The current literature has provided enough evidence that the reaction time needed to degrade the target pharmaceuticals completely is insufficient for the complete mineralization. This ascertains that the parent compound has been converted majorly into the intermediates and will usually take more time to transform into harmless by-products.

The visible light photocatalytic degradation of pharmaceuticals typically fits the pseudo-first-order kinetic equation (Eq. 14) corresponding to the Langmuir–Hinshelwood model and is consistent with the current literature.

$$\ln\left(\frac{C_0}{C_t}\right) = kt \tag{14}$$

Thus, it has been observed that the photodegradation reaction rate is high at the beginning, and then it gradually slows down with the gradual increase in reaction time. The reason behind this can be the increasing competition with time between the parent organic molecules and the by-products and intermediates for the reactive sites on the surface of the photocatalyst.

Presence of ions and natural organic matter

The natural water resources, as well as industrial and domestic effluents, are enriched with inorganic ions that could influence the photocatalytic reaction in practical wastewater application. Inorganic anions such as $S_2O_8^{2-}$, BrO_3^-, and SO_3^- increase the photocatalytic degradation by scavenging e^-, thereby reducing e^-–h^+ recombination. However, excessive concentrations of inorganic species can suppress photodegradation by scavenging $^{\cdot}OH$. Inorganic ions, such as Cl^-, NO_3^-, SO_4^{2-}, HCO_3^-, and $H_2PO_4^-$, could act as h^+ and $^{\cdot}OH$ scavengers to form ionic radicals, which are weaker oxidizing agents than h^+ and $^{\cdot}OH$. Additionally, they adsorb on the catalyst surface and block active sites. As a result, the degradation efficiency is reduced in their presence. Reduction in the photodegradation efficiency of IBF (Wang et al. 2017a) and SNM (Wang et al. 2011b) due to the effect of inorganic ions has been reported.

Ionic strength is an important parameter controlling photocatalytic activity; at high ionic strength, the repulsive force of contaminants can be mitigated to enhance adsorption. Photodegradation of CA was inhibited at low concentrations of NaCl (< 10 g L^{-1}), while at higher concentrations (> 10 g L^{-1}) of NaCl the degradation efficiency was at par with that in pure water (Awfa et al. 2018). Similar results were observed during the photocatalytic degradation of TC (Wang et al. 2016a). Additionally, cations, for example, Na^+, may compete with the pollutants for the adsorption sites of photocatalyst with the increase in ionic strength, leading to the lowered photocatalytic efficiency (Chen et al. 2017). Chen et al. reported the significant inhibition of TC degradation by Ca^{2+} and Mg^{2+} (Chen and Liu 2016). On the other hand, Mn^{2+} increased the photo-oxidation by surface reaction, increasing the number of photogenerated e^- and h^+ and inhibiting e^-–h^+ recombination (Kabra et al. 2004).

Natural organic matter (NOM) present in natural water resources is scavengers of ROS. Wang et al. reported that the visible light degradation of IBF mixed in a raw water sample by photocatalyst UTCB-25 was subdued by the NOM present in the sample (Wang et al. 2017a).

Application in real field

The studies covered in this review are centered on laboratory-scale experiments. To the authors' knowledge, there is no report on pilot-scale or large-scale studies of visible light photocatalysts toward pharmaceutical removal. Reports of pharmaceutical removal from real wastewater are present though. Deng et al. used $Ag/AgIn_5S_8$ photocatalyst to degrade real pharmaceutical wastewater sample containing $COD_0 \sim 31{,}500$ mg L^{-1} under visible light and obtained a mineralization efficiency of 56.3% in 9 h and 77.6% COD removal efficiency in 12 h (Deng et al. 2018). Stability and recyclability of a photocatalyst are also important factors that influence its real field applications. Jiang et al. reported the superior stability of CN/K^+CNO^-, whose photocatalytic

efficiency remained unchanged after four repeated cycles of TC degradation (Jiang et al. 2017). To apply the technology in the real field, one has to look for technologically feasible, economically viable, and eco-friendly solutions. This can be achieved if the photocatalytic process has high degradation and mineralization efficiencies, non-toxic end products, fast kinetics, and a highly stable photocatalyst. The use of non-toxic photocatalysts should be considered to avoid any risk to the environment and human health. For example, histopathological changes and oxidative stress have been observed in certain species of fish that were exposed to some transition metals-doped TiO_2 NPs commonly used as photocatalysts (Pirsaheb et al. 2019). In addition to this, the catalyst should be separated easily from the aqueous solution. Combining photocatalysis with other treatment processes may lead to an economical and efficient way toward its practical application. For example, Yahiat et al. reported some success with a hybrid process combining UV light photocatalysis with biological treatment (Yahiat et al. 2011). Although a combined treatment process integrating visible light photocatalysis and other methods is yet to be reported. Additionally, the efficient use of solar light will make the process an economical, sustainable, and green solution for water treatment.

Issues and challenges

Among the various AOPs, the visible-light-assisted photocatalysis has become a popular technique for the removal of pharmaceutical pollutants. Despite several benefits of this technique as discussed earlier, several issues have been identified from the critical review of the current literature that can be seen as prospective research opportunities:

- The single-component semiconductor photocatalysts have some inherent disadvantages which can be dealt with by suitably modifying them. However, it is interesting to see whether applying multiple modifications may lead to higher photocatalytic efficiency, which is the scope for future research.
- To enhance the photocatalytic efficiency and minimize the cost, the multivariate optimization of synthesis process of the photocatalyst is an essential requirement, although significant attention in this context is rarely provided.
- Apart from the photocatalytic efficiency, the stability and recyclability of a photocatalyst including its ease of separation from aqueous solutions are important considerations for its practical applications, which should be focused for promising future of photocatalysis in field-based treatment systems.
- Only a few studies have reported the role of influential parameters, such as light, pH, photocatalyst dosage, pollutant concentration, different ions, and NOMs, on the visible light photocatalysis of pharmaceuticals. However, this area needs sufficient attention to ascertain the photocatalytic treatment process of real wastewater.
- The existing literature for visible-light-assisted photocatalysis of pharmaceuticals mostly focused on antibiotics, especially the tetracycline group. Many therapeutic groups of pharmaceuticals remain unattended till date.
- More research is needed on visible light photocatalysis of pharmaceutical mixtures, as the composition of real wastewater is rarely constituted with single pollutant.
- Studies on continuous mode of operation for photocatalytic treatment system are rarely conducted, although it is an essential requirement for field-based treatment system.
- Conventional treatment methods can also be combined with the visible light photocatalysis to deliver a technically feasible and economically viable solution for pharmaceutical wastewater treatment, which needs to be adequately explored.

Extensive research may be carried out in the application of photocatalytic degradation of pharmaceutical pollutants, which in turn may evolve the opportunity to explore the future of this promising technology in the arena of environmental remediation.

Conclusion

The present review focuses on the recent advancement of visible-light-assisted photocatalysis for pharmaceutical removal. Semiconductor photocatalysis using visible light has shown tremendous potential as a highly efficient technique to treat pharmaceuticals and protect the environment. The current review has covered the important aspects of pharmaceutical pollutants, including a concise overview of their occurrence, fate, and harmful effects on the environment and health, stressing on the significant need for its removal from the contaminated water. The fundamentals and detailed mechanism of semiconductor photocatalysis have been focused along with a brief discussion on various removal technologies. A detailed report on the recent developments of various visible-light-active photocatalysts for the removal of pharmaceuticals, used with or without modifications and supports, their detailed mechanisms, the role of influential parameters such as light and pH, and their potential practical applications, is certainly the main focus of this review. Overall, the reported visible-light-active photocatalysts have shown tremendous potential for practical applications toward the degradation and mineralization of

pharmaceutical pollutants. This review, covering a comprehensive update of the present research, will fuel new interest in the development of more efficient and practical applications for the photocatalytic removal of pharmaceuticals, as well as catalyze the research on the remediation of emerging contaminants in a pragmatic approach.

Acknowledgements Authors express their gratitude to the Ministry of Human Resource Development, Government of India, for financial support. We also gratefully acknowledge the help of Prof. Tarasankar Pal (Department of Chemistry, IIT Kharagpur) and Mr. Ashish Kumar Nayak (Department of Civil Engineering, IIT Kharagpur).

Compliance with ethical standards

Conflict of interest The authors declare that there are no conflicts of interests.

References

Ai C, Zhou D, Wang Q et al (2015) Optimization of operating parameters for photocatalytic degradation of tetracycline using In_2S_3 under natural solar radiation. Sol Energy 113:34–42. https://doi.org/10.1016/j.solener.2014.12.022

Awfa D, Ateia M, Fujii M et al (2018) Photodegradation of pharmaceuticals and personal care products in water treatment using carbonaceous-TiO_2 composites: a critical review of recent literature. Water Res 142:26–45. https://doi.org/10.1016/j.watres.2018.05.036

Azimi S, Nezamzadeh-Ejhieh A (2015) Enhanced activity of clinoptilolite-supported hybridized PbS–CdS semiconductors for the photocatalytic degradation of a mixture of tetracycline and cephalexin aqueous solution. J Mol Catal A Chem 408:152–160. https://doi.org/10.1016/j.molcata.2015.07.017

Babuponnusami A, Muthukumar K (2014) A review on Fenton and improvements to the Fenton process for wastewater treatment. J Environ Chem Eng 2:557–572. https://doi.org/10.1016/j.jece.2013.10.011

Bai Y-Y, Wang F-R, Liu J-K (2016) A new complementary catalyst and catalytic mechanism: Ag_2MoO_4/Ag/AgBr/GO heterostructure. Ind Eng Chem Res 55:9873–9879. https://doi.org/10.1021/acs.iecr.6b01265

Belver C, Bedia J, Rodriguez JJ (2017) Zr-doped TiO_2 supported on delaminated clay materials for solar photocatalytic treatment of emerging pollutants. J Hazard Mater 322:233–242. https://doi.org/10.1016/j.jhazmat.2016.02.028

Bengtsson-Palme J, Boulund F, Fick J et al (2014) Shotgun metagenomics reveals a wide array of antibiotic resistance genes and mobile elements in a polluted lake in India. Front Microbiol 5:648

Besse JP, Garric J (2008) Human pharmaceuticals in surface waters. Implementation of a prioritization methodology and application to the French situation. Toxicol Lett 176:104–123. https://doi.org/10.1016/j.toxlet.2007.10.012

Bian ZY, Zhu YQ, Zhang JX et al (2014) Visible-light driven degradation of ibuprofen using abundant metal-loaded $BiVO_4$ photocatalysts. Chemosphere 117:527–531. https://doi.org/10.1016/j.chemosphere.2014.09.017

Bilgin Simsek E (2017) Solvothermal synthesized boron doped TiO_2 catalysts: photocatalytic degradation of endocrine disrupting compounds and pharmaceuticals under visible light irradiation. Appl Catal B Environ 200:309–322. https://doi.org/10.1016/j.apcatb.2016.07.016

Bo L, He K, Tan N et al (2017) Photocatalytic oxidation of trace carbamazepine in aqueous solution by visible-light-driven $Znln_2S_4$: performance and mechanism. J Environ Manag 190:259–265. https://doi.org/10.1016/j.jenvman.2016.12.050

Borges ME, Hernández T, Esparza P (2014) Photocatalysis as a potential tertiary treatment of urban wastewater: new photocatalytic materials. Clean Technol Environ Policy 16:431–436. https://doi.org/10.1007/s10098-013-0637-z

Bound JP, Kitsou K, Voulvoulis N (2006) Household disposal of pharmaceuticals and perception of risk to the environment. Environ Toxicol Pharmacol 21:301–307. https://doi.org/10.1016/j.etap.2005.09.006

Boxi SS, Paria S (2015) Visible light induced enhanced photocatalytic degradation of organic pollutants in aqueous media using Ag doped hollow TiO_2 nanospheres. RSC Adv 5:37657–37668. https://doi.org/10.1039/C5RA03421C

Byrne JA, Dunlop PSM, Hamilton JWJ et al (2015) A review of heterogeneous photocatalysis for water and surface disinfection. Molecules 20:5574–5615. https://doi.org/10.3390/molecules20045574

Cai F, Tang Y, Chen F et al (2015) Enhanced visible-light-driven photocatalytic degradation of tetracycline by Cr^{3+} doping $SrTiO_3$ cubic nanoparticles. RSC Adv 5:21290–21296. https://doi.org/10.1039/C4RA13821J

Cao Q, Yu Q, Connell DW, Yu G (2013) Titania/carbon nanotube composite (TiO_2/CNT) and its application for removal of organic pollutants. Clean Technol Environ Policy 15:871–880. https://doi.org/10.1007/s10098-013-0581-y

Cao M, Wang P, Ao Y et al (2016) Visible light activated photocatalytic degradation of tetracycline by a magnetically separable composite photocatalyst: graphene oxide/magnetite/cerium-doped titania. J Colloid Interface Sci 467:129–139. https://doi.org/10.1016/j.jcis.2016.01.005

Chen M, Chu W (2015) Photocatalytic degradation and decomposition mechanism of fluoroquinolones norfloxacin over bismuth tungstate: experiment and mathematic model. Appl Catal B Environ 168–169:175–182. https://doi.org/10.1016/j.apcatb.2014.12.023

Chen Y, Liu K (2016) Preparation and characterization of nitrogen-doped TiO_2/diatomite integrated photocatalytic pellet for the adsorption–degradation of tetracycline hydrochloride using visible light. Chem Eng J 302:682–696. https://doi.org/10.1016/j.cej.2016.05.108

Chen Q, Wu S, Xin Y (2016) Synthesis of Au–CuS–TiO_2 nanobelts photocatalyst for efficient photocatalytic degradation of antibiotic oxytetracycline. Chem Eng J 302:377–387. https://doi.org/10.1016/j.cej.2016.05.076

Chen F, Yang Q, Li X et al (2017) Hierarchical assembly of graphene-bridged Ag_3PO_4/Ag/$BiVO_4$ (040) Z-scheme photocatalyst: an efficient, sustainable and heterogeneous catalyst with enhanced visible-light photoactivity towards tetracycline degradation under visible light irradiation. Appl Catal B Environ 200:330–342. https://doi.org/10.1016/j.apcatb.2016.07.021

Chen M, Yao J, Huang Y et al (2018) Enhanced photocatalytic degradation of ciprofloxacin over Bi_2O_3/$(BiO)_2CO_3$ heterojunctions: efficiency, kinetics, pathways, mechanisms and toxicity evaluation. Chem Eng J 334:453–461. https://doi.org/10.1016/j.cej.2017.10.064

Cheng H, Hou J, Takeda O et al (2015) A unique Z-scheme 2D/2D nanosheet heterojunction design to harness charge transfer for photocatalysis. J Mater Chem A 3:11006–11013. https://doi.org/10.1039/C5TA01864A

Chong MN, Jin B, Chow CWK, Saint C (2010) Recent developments in photocatalytic water treatment technology: a review. Water Res 44:2997–3027. https://doi.org/10.1016/j.watres.2010.02.039

Chu X, Shan G, Chang C et al (2016) Effective degradation of tetracycline by mesoporous Bi_2WO_6 under visible light irradiation. Front Environ Sci Eng 10:211–218. https://doi.org/10.1007/s11783-014-0753-y

Cleuvers M (2003) Aquatic ecotoxicity of pharmaceuticals including the assessment of combination effects. Toxicol Lett 142:185–194. https://doi.org/10.1016/S0378-4274(03)00068-7

Cui Y, Ma Q, Deng X et al (2017) Fabrication of Ag–Ag_2O/reduced TiO_2 nanophotocatalyst and its enhanced visible light driven photocatalytic performance for degradation of diclofenac solution. Appl Catal B Environ 206:136–145. https://doi.org/10.1016/j.apcatb.2017.01.014

De Andrade JR, Oliveira MF, Da Silva MGC, Vieira MGA (2018) Adsorption of pharmaceuticals from water and wastewater using nonconventional low-cost materials: a review. Ind Eng Chem Res 57:3103–3127. https://doi.org/10.1021/acs.iecr.7b05137

Debnath D, Gupta AK, Ghosal PS (2018) Recent advances in the development of tailored functional materials for the treatment of pesticides in aqueous media: a review. J Ind Eng Chem. https://doi.org/10.1016/J.JIEC.2018.10.014

Deng F, Zhao L, Luo X et al (2018) Highly efficient visible-light photocatalytic performance of Ag/$AgIn_5S_8$ for degradation of tetracycline hydrochloride and treatment of real pharmaceutical industry wastewater. Chem Eng J 333:423–433. https://doi.org/10.1016/j.cej.2017.09.022

Di J, Xia J, Ge Y et al (2015) Novel visible-light-driven CQDs/Bi_2WO_6 hybrid materials with enhanced photocatalytic activity toward organic pollutants degradation and mechanism insight. Appl Catal B Environ 168–169:51–61. https://doi.org/10.1016/j.apcatb.2014.11.057

Dietrich S, Ploessl F, Bracher F, Laforsch C (2010) Single and combined toxicity of pharmaceuticals at environmentally relevant concentrations in *Daphnia magna*—a multigenerational study. Chemosphere 79:60–66. https://doi.org/10.1016/j.chemosphere.2009.12.069

Ding Y, Zhang G, Wang X et al (2017) Chemical and photocatalytic oxidative degradation of carbamazepine by using metastable Bi^{3+} self-doped $NaBiO_3$ nanosheets as a bifunctional material. Appl Catal B Environ 202:528–538. https://doi.org/10.1016/j.apcatb.2016.09.054

Dong Z, Senn DB, Moran RE, Shine JP (2013) Prioritizing environmental risk of prescription pharmaceuticals. Regul Toxicol Pharmacol 65:60–67. https://doi.org/10.1016/j.yrtph.2012.07.003

Dong S, Feng J, Fan M et al (2015) Recent developments in heterogeneous photocatalytic water treatment using visible light-responsive photocatalysts: a review. RSC Adv 5:14610–14630. https://doi.org/10.1039/C4RA13734E

Fujishima A, Honda K (1972) Electrochemical photolysis of water at a semiconductor electrode. Nature 238:37–38. https://doi.org/10.1038/238037a0

Ganiyu SO, Van Hullebusch ED, Cretin M et al (2015) Coupling of membrane filtration and advanced oxidation processes for removal of pharmaceutical residues: a critical review. Sep Purif Technol 156:891–914. https://doi.org/10.1016/j.seppur.2015.09.059

Gao X, Zhang X, Wang Y et al (2015) Rapid synthesis of hierarchical BiOCl microspheres for efficient photocatalytic degradation of carbamazepine under simulated solar irradiation. Chem Eng J 263:419–426. https://doi.org/10.1016/j.cej.2014.10.110

Gautam S, Shandilya P, Singh VP et al (2016) Solar photocatalytic mineralization of antibiotics using magnetically separable $NiFe_2O_4$ supported onto graphene sand composite and bentonite. J Water Process Eng 14:86–100. https://doi.org/10.1016/j.jwpe.2016.10.008

Gautam S, Shandilya P, Priya B et al (2017) Superparamagnetic $MnFe_2O_4$ dispersed over graphitic carbon sand composite and bentonite as magnetically recoverable photocatalyst for antibiotic mineralization. Sep Purif Technol 172:498–511. https://doi.org/10.1016/j.seppur.2016.09.006

Gaya UI, Abdullah AH (2008) Heterogeneous photocatalytic degradation of organic contaminants over titanium dioxide: a review of fundamentals, progress and problems. J Photochem Photobiol C Photochem Rev 9:1–12. https://doi.org/10.1016/j.jphotochemrev.2007.12.003

Gunnarsson L, Kristiansson E, Rutgersson C et al (2009) Pharmaceutical industry effluent diluted 1:500 affects global gene expression, cytochrome P450 1A activity, and plasma phosphate in fish. Environ Toxicol Chem 28:2639–2647. https://doi.org/10.1897/09-120.1

Hailili R, Wang Z-Q, Xu M et al (2017) Layered nanostructured ferroelectric perovskite $Bi_5FeTi_3O_{15}$ for visible light photodegradation of antibiotics. J Mater Chem A 5:21275–21290. https://doi.org/10.1039/C7TA06618J

Hailili R, Wang ZQ, Li Y et al (2018) Oxygen vacancies induced visible-light photocatalytic activities of $CaCu_3Ti_4O_{12}$ with controllable morphologies for antibiotic degradation. Appl Catal B Environ 221:422–432. https://doi.org/10.1016/j.apcatb.2017.09.026

Halling-Sørensen B, Nors Nielsen S, Lanzky PF et al (1998) Occurrence, fate and effects of pharmaceutical substances in the environment—a review. Chemosphere 36:357–393. https://doi.org/10.1016/S0045-6535(97)00354-8

Han C, Likodimos V, Khan JA et al (2013) UV–visible light-activated Ag-decorated, monodisperse TiO_2 aggregates for treatment of the pharmaceutical oxytetracycline. Environ Sci Pollut Res 21:11781–11793. https://doi.org/10.1007/s11356-013-2233-5

Hao R, Xiao X, Zuo X et al (2012) Efficient adsorption and visible-light photocatalytic degradation of tetracycline hydrochloride using mesoporous BiOI microspheres. J Hazard Mater 209–210:137–145. https://doi.org/10.1016/j.jhazmat.2012.01.006

Hernández-Uresti DB, Vázquez A, Sanchez-Martinez D, Obregón S (2016) Performance of the polymeric g-C_3N_4 photocatalyst through the degradation of pharmaceutical pollutants under UV–vis irradiation. J Photochem Photobiol A Chem 324:47–52. https://doi.org/10.1016/j.jphotochem.2016.01.031

Homem V, Santos L (2011) Degradation and removal methods of antibiotics from aqueous matrices—a review. J Environ Manag 92:2304–2347. https://doi.org/10.1016/j.jenvman.2011.05.023

Hong Y, Ren A, Jiang Y et al (2015) Sol–gel synthesis of visible-light-driven $Ni_{(1-x)}Cu_{(x)}Fe_2O_4$ photocatalysts for degradation of tetracycline. Ceram Int 41:1477–1486. https://doi.org/10.1016/j.ceramint.2014.09.082

Hong Y, Li C, Zhang G et al (2016) Efficient and stable Nb_2O_5 modified g-C_3N_4 photocatalyst for removal of antibiotic pollutant. Chem Eng J 299:74–84. https://doi.org/10.1016/j.cej.2016.04.092

Hong Y, Li C, Yin B et al (2018) Promoting visible-light-induced photocatalytic degradation of tetracycline by an efficient and stable beta-Bi_2O_3@g-C_3N_4 core/shell nanocomposite. Chem Eng J 338:137–146. https://doi.org/10.1016/j.cej.2017.12.108

Ikehata K, Jodeiri Naghashkar N, Gamal El-Din M (2006) Degradation of aqueous pharmaceuticals by ozonation and advanced oxidation processes: a review. Ozone Sci Eng J Int Ozone Assoc 28:353–414. https://doi.org/10.1080/01919510600985937

Jesudoss SK, Vijaya JJ, Selvam NCS et al (2016) Effects of Ba doping on structural, morphological, optical, and photocatalytic properties of self-assembled ZnO nanospheres. Clean Technol Environ Policy 18:729–741. https://doi.org/10.1007/s10098-015-1047-1

Ji M, Di J, Ge Y et al (2017) 2D–2D stacking of graphene-like g-C3N4/ultrathin $Bi_4O_5Br_2$ with matched energy band structure towards

antibiotic removal. Appl Surf Sci 413:372–380. https://doi.org/10.1016/j.apsusc.2017.03.287

Jiang D, Wang T, Xu Q et al (2017) Perovskite oxide ultrathin nanosheets/g-C_3N_4 2D–2D heterojunction photocatalysts with significantly enhanced photocatalytic activity towards the photodegradation of tetracycline. Appl Catal B Environ 201:617–628. https://doi.org/10.1016/j.apcatb.2016.09.001

Jiang D, Wen B, Xu Q et al (2018) Plasmonic Au nanoparticles/$KCa_2Nb_3O_{10}$ nanosheets 0D/2D heterojunctions with enhanced photocatalytic activity towards the degradation of tetracycline hydrochloride. J Alloys Compd 762:38–45. https://doi.org/10.1016/j.jallcom.2018.05.178

Kabra K, Chaudhary R, Sawhney RL (2004) Treatment of hazardous organic and inorganic compounds through aqueous-phase photocatalysis: a review. Ind Eng Chem Res 43:7683–7696. https://doi.org/10.1021/ie0498551

Kanakaraju D, Glass BD, Oelgemöller M (2014) Titanium dioxide photocatalysis for pharmaceutical wastewater treatment. Environ Chem Lett 12:27–47. https://doi.org/10.1007/s10311-013-0428-0

Kanakaraju D, Glass BD, Oelgem M (2018) Advanced oxidation process-mediated removal of pharmaceuticals from water: a review. J Environ Manag 219:189–207. https://doi.org/10.1016/j.jenvman.2018.04.103

Karthik R, Vinoth Kumar J, Chen SM et al (2017) A study of electrocatalytic and photocatalytic activity of cerium molybdate nanocubes decorated graphene oxide for the sensing and degradation of antibiotic drug chloramphenicol. ACS Appl Mater Interfaces 9:6547–6559. https://doi.org/10.1021/acsami.6b14242

Khan MR, Chuan TW, Yousuf A et al (2015) Schottky barrier and surface plasmonic resonance phenomena towards the photocatalytic reaction: study of their mechanisms to enhance photocatalytic activity. Catal Sci Technol 5:2522–2531. https://doi.org/10.1039/C4CY01545B

Klavarioti M, Mantzavinos D, Kassinos D (2009) Removal of residual pharmaceuticals from aqueous systems by advanced oxidation processes. Environ Int 35:402–417. https://doi.org/10.1016/j.envint.2008.07.009

Kosma CI, Lambropoulou DA, Albanis TA (2014) Investigation of PPCPs in wastewater treatment plants in Greece: occurrence, removal and environmental risk assessment. Sci Total Environ 466–467:421–438. https://doi.org/10.1016/j.scitotenv.2013.07.044

Kumar A, Kumar A, Sharma G et al (2018) Quaternary magnetic BiOCl/g-C_3N_4/Cu_2O/Fe_3O_4 nano-junction for visible light and solar powered degradation of sulfamethoxazole from aqueous environment. Chem Eng J 334:462–478. https://doi.org/10.1016/j.cej.2017.10.049

Kummerer K (2001) Drugs in the environment: emission of drugs, diagnostic aids and disinfectants into wastewater by hospitals in relation to other sources—a review. Chemosphere 45:957–969. https://doi.org/10.1016/S0045-6535(01)00144-8

Kyzas GZ, Fu J, Lazaridis NK et al (2015) New approaches on the removal of pharmaceuticals from wastewaters with adsorbent materials. J Mol Liq 209:87–93. https://doi.org/10.1016/j.molliq.2015.05.025

Lang X, Chen X, Zhao J (2014) Heterogeneous visible light photocatalysis for selective organic transformations. Chem Soc Rev 43:473–486. https://doi.org/10.1039/C3CS60188A

Larsson DGJ (2010) Release of active pharmaceutical ingredients from manufacturing sites—need for new management strategies. Integr Environ Assess Manag 6:184–186. https://doi.org/10.1002/ieam.20

Larsson DGJ, de Pedro C, Paxeus N (2007) Effluent from drug manufactures contains extremely high levels of pharmaceuticals. J Hazard Mater 148:751–755. https://doi.org/10.1016/j.jhazmat.2007.07.008

Lei Z, Wang J, Wang L et al (2016) Efficient photocatalytic degradation of ibuprofen in aqueous solution using novel visible-light responsive graphene quantum dot/$AgVO_3$ nanoribbons. J Hazard Mater 312:298–306. https://doi.org/10.1016/j.jhazmat.2016.03.044

Leong S, Li D, Hapgood K et al (2016) $Ni(OH)_2$ decorated rutile TiO_2 for efficient removal of tetracycline from wastewater. Appl Catal B Environ 198:224–233. https://doi.org/10.1016/j.apcatb.2016.05.043

Li P, Liu C, Wu G et al (2014) Solvothermal synthesis and visible light-driven photocatalytic degradation for tetracycline of Fe-doped $SrTiO_3$. RSC Adv 4:47615–47624. https://doi.org/10.1039/C4RA06630H

Li F, Kang Y, Chen M et al (2016a) Photocatalytic degradation and removal mechanism of ibuprofen via monoclinic $BiVO_4$ under simulated solar light. Chemosphere 150:139–144. https://doi.org/10.1016/j.chemosphere.2016.02.045

Li J, Sun S, Qian C et al (2016b) The role of adsorption in photocatalytic degradation of ibuprofen under visible light irradiation by BiOBr microspheres. Chem Eng J 297:139–147. https://doi.org/10.1016/j.cej.2016.03.145

Lin CJ, Yang WT (2013) Ordered mesostructured Cu-doped TiO_2 spheres as active visible-light-driven photocatalysts for degradation of paracetamol. Chem Eng J 237:131–137. https://doi.org/10.1016/j.cej.2013.10.027

Lin L, Wang H, Jiang W et al (2017a) Comparison study on photocatalytic oxidation of pharmaceuticals by TiO_2–Fe and TiO_2-reduced graphene oxide nanocomposites immobilized on optical fibers. J Hazard Mater 333:162–168. https://doi.org/10.1016/j.jhazmat.2017.02.044

Lin L, Wang H, Xu P (2017b) Immobilized TiO_2-reduced graphene oxide nanocomposites on optical fibers as high performance photocatalysts for degradation of pharmaceuticals. Chem Eng J 310:389–398. https://doi.org/10.1016/j.cej.2016.04.024

Liu C, Wu G, Chen J et al (2016a) Fabrication of a visible-light-driven photocatalyst and degradation of tetracycline based on the photoinduced interfacial charge transfer of $SrTiO_3$/Fe_2O_3 nanowires. New J Chem 40:5198–5208. https://doi.org/10.1039/C5NJ03167B

Liu M, Hou L, Xi B et al (2016b) Magnetically separable Ag/AgCl-zero valent iron particles modified zeolite X heterogeneous photocatalysts for tetracycline degradation under visible light. Chem Eng J 302:475–484. https://doi.org/10.1016/j.cej.2016.05.083

Low J, Cheng B, Yu J (2017) Surface modification and enhanced photocatalytic CO_2 reduction performance of TiO_2: a review. Appl Surf Sci 392:658–686. https://doi.org/10.1016/J.APSUSC.2016.09.093

Luo B, Xu D, Li D et al (2015) Fabrication of a Ag/Bi_3TaO_7 plasmonic photocatalyst with enhanced photocatalytic activity for degradation of tetracycline. ACS Appl Mater Interfaces 7:17061–17069. https://doi.org/10.1021/acsami.5b03535

Ma X, Jiang D, Xiao P et al (2017) 2D/2D heterojunctions of WO_3 nanosheet/$K^+Ca_2Nb_3O_{10}^-$ ultrathin nanosheet with improved charge separation efficiency for significantly boosting photocatalysis. Catal Sci Technol 7:3481–3491. https://doi.org/10.1039/C7CY00976C

Maeda K (2011) Photocatalytic water splitting using semiconductor particles: history and recent developments. J Photochem Photobiol C Photochem Rev 12:237–268. https://doi.org/10.1016/j.jphotochemrev.2011.07.001

Mahamallik P, Saha S, Pal A (2015) Tetracycline degradation in aquatic environment by highly porous MnO_2 nanosheet assembly. Chem Eng J 276:155–165. https://doi.org/10.1016/j.cej.2015.04.064

Mahmoud WMM, Rastogi T, Kümmerer K (2017) Application of titanium dioxide nanoparticles as a photocatalyst for the removal of micropollutants such as pharmaceuticals from water. Curr Opin

Green Sustain Chem 6:1–10. https://doi.org/10.1016/j.cogsc.2017.04.001

Martinez JL (2009) Environmental pollution by antibiotics and by antibiotic resistance determinants. Environ Pollut 157:2893–2902. https://doi.org/10.1016/j.envpol.2009.05.051

Miklos DB, Remy C, Jekel M et al (2018) Evaluation of advanced oxidation processes for water and wastewater treatment—a critical review. Water Res 139:118–131. https://doi.org/10.1016/j.watres.2018.03.042

Mirzaei A, Chen Z, Haghighat F, Yerushalmi L (2016) Removal of pharmaceuticals and endocrine disrupting compounds from water by zinc oxide-based photocatalytic degradation: a review. Sustain Cities Soc 27:407–418. https://doi.org/10.1016/J.SCS.2016.08.004

Mirzaei A, Chen Z, Haghighat F, Yerushalmi L (2017) Removal of pharmaceuticals from water by homo/heterogonous Fenton-type processes—a review. Chemosphere 174:665–688. https://doi.org/10.1016/j.chemosphere.2017.02.019

Natarajan TS, Thampi KR, Tayade RJ (2018) Visible light driven redox-mediator-free dual semiconductor photocatalytic systems for pollutant degradation and the ambiguity in applying Z-scheme concept. Appl Catal B Environ 227:296–311. https://doi.org/10.1016/j.apcatb.2018.01.015

Niu J, Ding S, Zhang L et al (2013) Visible-light-mediated Sr-Bi_2O_3 photocatalysis of tetracycline: kinetics, mechanisms and toxicity assessment. Chemosphere 93:1–8. https://doi.org/10.1016/j.chemosphere.2013.04.043

Oller I, Malato S, Sánchez-Pérez JA (2011) Combination of advanced oxidation processes and biological treatments for wastewater decontamination—a review. Sci Total Environ 409:4141–4166. https://doi.org/10.1016/j.scitotenv.2010.08.061

Omorogie MO, Ofomaja AE (2017) Clean technology and response surface approach for the photodegradation of selected antibiotics by catalyst supported on pine activated carbon. Clean Technol Environ Policy 19:2191–2213. https://doi.org/10.1007/s10098-017-1411-4

Onesios KM, Yu JT, Bouwer EJ (2009) Biodegradation and removal of pharmaceuticals and personal care products in treatment systems: a review. Biodegradation 20:441–466. https://doi.org/10.1007/s10532-008-9237-8

Ortiz de García SA, Pinto Pinto G, García-Encina PA, Irusta-Mata R (2014) Ecotoxicity and environmental risk assessment of pharmaceuticals and personal care products in aquatic environments and wastewater treatment plants. Ecotoxicology 23:1517–1533. https://doi.org/10.1007/s10646-014-1293-8

Palominos RA, Mondaca MA, Giraldo A et al (2009) Photocatalytic oxidation of the antibiotic tetracycline on TiO_2 and ZnO suspensions. Catal Today 144:100–105. https://doi.org/10.1016/j.cattod.2008.12.031

Panneri S, Ganguly P, Mohan M et al (2017) Photoregenerable, bifunctional granules of carbon-doped g-C_3N_4 as adsorptive photocatalyst for the efficient removal of tetracycline antibiotic. ACS Sustain Chem Eng 5:1610–1618. https://doi.org/10.1021/acssuschemeng.6b02383

Pelaez M, Nolan NT, Pillai SC et al (2012) A review on the visible light active titanium dioxide photocatalysts for environmental applications. Appl Catal B Environ 125:331–349. https://doi.org/10.1016/j.apcatb.2012.05.036

Pereira JHOS, Vilar VJP, Borges MT et al (2011) Photocatalytic degradation of oxytetracycline using TiO_2 under natural and simulated solar radiation. Sol Energy 85:2732–2740. https://doi.org/10.1016/j.solener.2011.08.012

Pirsaheb M, Azadi NA, Miglietta ML et al (2019) Toxicological effects of transition metal-doped titanium dioxide nanoparticles on goldfish (*Carassius auratus*) and common carp (*Cyprinus carpio*). Chemosphere 215:904–915. https://doi.org/10.1016/j.chemosphere.2018.10.111

Priya B, Raizada P, Singh N et al (2016a) Adsorptional photocatalytic mineralization of oxytetracycline and ampicillin antibiotics using Bi_2O_3/BiOCl supported on graphene sand composite and chitosan. J Colloid Interface Sci 479:271–283. https://doi.org/10.1016/j.jcis.2016.06.067

Priya B, Shandilya P, Raizada P et al (2016b) Photocatalytic mineralization and degradation kinetics of ampicillin and oxytetracycline antibiotics using graphene sand composite and chitosan supported BiOCl. J Mol Catal A Chem 423:400–413. https://doi.org/10.1016/j.molcata.2016.07.043

Ray C, Pal T (2017) Recent advances of metal–metal oxide nanocomposites and their tailored nanostructures in numerous catalytic applications. J Mater Chem A 5:9465–9487. https://doi.org/10.1039/C7TA02116J

Ren A, Liu C, Hong Y et al (2014) Enhanced visible-light-driven photocatalytic activity for antibiotic degradation using magnetic $NiFe_2O_4$/Bi_2O_3 heterostructures. Chem Eng J 258:301–308. https://doi.org/10.1016/j.cej.2014.07.071

Rivera-Utrilla J, Sánchez-Polo M, Ferro-García MÁ et al (2013) Pharmaceuticals as emerging contaminants and their removal from water. A review. Chemosphere 93:1268–1287. https://doi.org/10.1016/j.chemosphere.2013.07.059

Robles-Molina J, Gilbert-López B, García-Reyes JF, Molina-Díaz A (2014) Monitoring of selected priority and emerging contaminants in the Guadalquivir River and other related surface waters in the province of Jaén, South East Spain. Sci Total Environ 479–480:247–257. https://doi.org/10.1016/j.scitotenv.2014.01.121

Safari GH, Hoseini M, Seyedsalehi M et al (2014) Photocatalytic degradation of tetracycline using nanosized titanium dioxide in aqueous solution. Int J Environ Sci Technol 12:603–616. https://doi.org/10.1007/s13762-014-0706-9

Serpone N, Artemev YM, Ryabchuk VK et al (2017) Light-driven advanced oxidation processes in the disposal of emerging pharmaceutical contaminants in aqueous media: a brief review. Curr Opin Green Sustain Chem 6:18–33. https://doi.org/10.1016/j.cogsc.2017.05.003

Shi JW, Wang Z, He C et al (2015) CdS quantum dots modified N-doped titania plates for the photocatalytic mineralization of diclofenac in water under visible light irradiation. J Mol Catal A Chem 399:79–85. https://doi.org/10.1016/j.molcata.2015.01.030

Shi Y, Yang Z, Wang B et al (2016) Adsorption and photocatalytic degradation of tetracycline hydrochloride using a palygorskite-supported Cu_2O–TiO_2 composite. Appl Clay Sci 119:311–320. https://doi.org/10.1016/j.clay.2015.10.033

Sirés I, Brillas E, Oturan MA et al (2014) Electrochemical advanced oxidation processes: today and tomorrow. A review. Environ Sci Pollut Res 21:8336–8367. https://doi.org/10.1007/s11356-014-2783-1

Sood S, Mehta SK, Sinha ASK, Kansal SK (2016) Bi_2O_3/TiO_2 heterostructures: synthesis, characterization and their application in solar light mediated photocatalyzed degradation of an antibiotic, ofloxacin. Chem Eng J 290:45–52. https://doi.org/10.1016/j.cej.2016.01.017

Stackelberg PE, Gibs J, Furlong ET et al (2007) Efficiency of conventional drinking-water-treatment processes in removal of pharmaceuticals and other organic compounds. Sci Total Environ 377:255–272. https://doi.org/10.1016/j.scitotenv.2007.01.095

Sturini M, Speltini A, Maraschi F et al (2017) g-C_3N_4-promoted degradation of ofloxacin antibiotic in natural waters under simulated sunlight. Environ Sci Pollut Res 24:4153–4161. https://doi.org/10.1007/s11356-016-8156-1

Tang Y, Liu X, Ma C et al (2015) Enhanced photocatalytic degradation of tetracycline antibiotics by reduced graphene oxide–CdS/ZnS heterostructure photocatalysts. New J Chem 39:5150–5160. https://doi.org/10.1039/C5NJ00681C

Vaiano V, Sacco O, Sannino D, Ciambelli P (2015) Photocatalytic removal of spiramycin from wastewater under visible light with N-doped TiO_2 photocatalysts. Chem Eng J 261:3–8. https://doi.org/10.1016/j.cej.2014.02.071

Verlicchi P, Al Aukidy M, Zambello E (2012) Occurrence of pharmaceutical compounds in urban wastewater: removal, mass load and environmental risk after a secondary treatment—a review. Sci Total Environ 429:123–155. https://doi.org/10.1016/j.scitotenv.2012.04.028

Wang P, Yap PS, Lim TT (2011a) C–N–S tridoped TiO_2 for photocatalytic degradation of tetracycline under visible-light irradiation. Appl Catal A Gen 399:252–261. https://doi.org/10.1016/j.apcata.2011.04.008

Wang P, Zhou T, Wang R, Lim TT (2011b) Carbon-sensitized and nitrogen-doped TiO_2 for photocatalytic degradation of sulfanilamide under visible-light irradiation. Water Res 45:5015–5026. https://doi.org/10.1016/j.watres.2011.07.002

Wang X, Tang Y, Chen Z, Lim TT (2012) Highly stable heterostructured Ag–AgBr/TiO_2 composite: a bifunctional visible-light active photocatalyst for destruction of ibuprofen and bacteria. J Mater Chem 22:23149–23158. https://doi.org/10.1039/c2jm35503e

Wang H, Yuan X, Wu Y et al (2016a) In situ synthesis of In_2S_3 at MIL-125(Ti) core-shell microparticle for the removal of tetracycline from wastewater by integrated adsorption and visible-light-driven photocatalysis. Appl Catal B Environ 186:19–29. https://doi.org/10.1016/j.apcatb.2015.12.041

Wang T, Quan W, Jiang D et al (2016b) Synthesis of redox-mediator-free direct Z-scheme AgI/WO_3 nanocomposite photocatalysts for the degradation of tetracycline with enhanced photocatalytic activity. Chem Eng J 300:280–290. https://doi.org/10.1016/j.cej.2016.04.128

Wang J, Tang L, Zeng G et al (2017a) Atomic scale g-C_3N_4/Bi_2WO_6 2D/2D heterojunction with enhanced photocatalytic degradation of ibuprofen under visible light irradiation. Appl Catal B Environ 209:285–294. https://doi.org/10.1016/j.apcatb.2017.03.019

Wang K, Zhang G, Li J et al (2017b) 0D/2D Z-Scheme heterojunctions of bismuth tantalate quantum dots/ultrathin g-C_3N_4 nanosheets for highly efficient visible light photocatalytic degradation of antibiotics. ACS Appl Mater Interfaces 9:43704–43715. https://doi.org/10.1021/acsami.7b14275

Wen XJ, Niu CG, Zhang L, Zeng GM (2017) Fabrication of SnO_2 nanopaticles/BiOI n–p heterostructure for wider spectrum visible-light photocatalytic degradation of antibiotic oxytetracycline hydrochloride. ACS Sustain Chem Eng 5:5134–5147. https://doi.org/10.1021/acssuschemeng.7b00501

Wu G, Li P, Xu D et al (2015) Hydrothermal synthesis and visible-light-driven photocatalytic degradation for tetracycline of Mn-doped $SrTiO_3$ nanocubes. Appl Surf Sci 333:39–47. https://doi.org/10.1016/j.apsusc.2015.02.008

Xia D, Lo IMC (2016) Synthesis of magnetically separable Bi_2O_4/Fe_3O_4 hybrid nanocomposites with enhanced photocatalytic removal of ibuprofen under visible light irradiation. Water Res 100:393–404. https://doi.org/10.1016/j.watres.2016.05.026

Xiao X, Hu R, Liu C et al (2013) Facile microwave synthesis of novel hierarchical $Bi_{24}O_{31}Br_{10}$ nanoflakes with excellent visible light photocatalytic performance for the degradation of tetracycline hydrochloride. Chem Eng J 225:790–797. https://doi.org/10.1016/j.cej.2013.03.103

Xu Q, Zhang L, Yu J et al (2018) Direct Z-scheme photocatalysts: principles, synthesis, and applications. Mater Today 21:1042–1063. https://doi.org/10.1016/j.mattod.2018.04.008

Xue J, Ma S, Zhou Y et al (2015a) Facile photochemical synthesis of Au/Pt/g-C_3N_4 with plasmon-enhanced photocatalytic activity for antibiotic degradation. ACS Appl Mater Interfaces 7:9630–9637. https://doi.org/10.1021/acsami.5b01212

Xue Z, Wang T, Chen B et al (2015b) Degradation of tetracycline with $BiFeO_3$ prepared by a simple hydrothermal method. Materials (Basel) 8:6360–6378. https://doi.org/10.3390/ma8095310

Yahiat S, Fourcade F, Brosillon S, Amrane A (2011) Removal of antibiotics by an integrated process coupling photocatalysis and biological treatment—case of tetracycline and tylosin. Int Biodeterior Biodegrad 65:997–1003. https://doi.org/10.1016/j.ibiod.2011.07.009

Yan M, Zhu F, Gu W et al (2016) Construction of nitrogen-doped graphene quantum dots-$BiVO_4$/g-C_3N_4 Z-scheme photocatalyst and enhanced photocatalytic degradation of antibiotics under visible light. RSC Adv 6:61162–61174. https://doi.org/10.1039/C6RA07589D

Yan M, Hua Y, Zhu F et al (2017a) Fabrication of nitrogen doped graphene quantum dots-BiOI/$MnNb_2O_6$ p–n junction photocatalysts with enhanced visible light efficiency in photocatalytic degradation of antibiotics. Appl Catal B Environ 202:518–527. https://doi.org/10.1016/j.apcatb.2016.09.039

Yan T, Wu T, Zhang Y et al (2017b) Fabrication of In_2S_3/Zn_2GeO_4 composite photocatalyst for degradation of acetaminophen under visible light. J Colloid Interface Sci 506:197–206. https://doi.org/10.1016/j.jcis.2017.06.079

Yang Y, Ok YS, Kim KH et al (2017) Occurrences and removal of pharmaceuticals and personal care products (PPCPs) in drinking water and water/sewage treatment plants: a review. Sci Total Environ 596–597:303–320. https://doi.org/10.1016/j.scitotenv.2017.04.102

You J, Xiang Y, Ge Y et al (2017) Synthesis of ternary rGO–ZnO–Fe_3O_4 nanocomposites and their application for visible light photocatalytic degradation of dyes. Clean Technol Environ Policy 19:2161–2169. https://doi.org/10.1007/s10098-017-1385-2

Yu S, Zhang Y, Dong F et al (2018) Readily achieving concentration-tunable oxygen vacancies in $Bi_2O_2CO_3$: triple-functional role for efficient visible-light photocatalytic redox performance. Appl Catal B Environ 226:441–450. https://doi.org/10.1016/j.apcatb.2017.12.074

Yuan F, Hu C, Hu X et al (2009) Degradation of selected pharmaceuticals in aqueous solution with UV and UV/H_2O_2. Water Res 43:1766–1774. https://doi.org/10.1016/J.watres.2009.01.008

Zhang G, Guan W, Shen H et al (2014) Organic additives-free hydrothermal synthesis and visible-light-driven photodegradation of tetracycline of WO_3 nanosheets. Ind Eng Chem Res 53:5443–5450. https://doi.org/10.1021/ie4036687

Zhang W, Zhou L, Deng H (2016) Ag modified g-C_3N_4 composites with enhanced visible-light photocatalytic activity for diclofenac degradation. J Mol Catal A Chem 423:270–276. https://doi.org/10.1016/j.molcata.2016.07.021

Zhao L, Deng J, Sun P et al (2018) Nanomaterials for treating emerging contaminants in water by adsorption and photocatalysis: systematic review and bibliometric analysis. Sci Total Environ 627:1253–1263. https://doi.org/10.1016/j.scitotenv.2018.02.006

Zhu XD, Wang YJ, Sun RJ, Zhou DM (2013) Photocatalytic degradation of tetracycline in aqueous solution by nanosized TiO_2. Chemosphere 92:925–932. https://doi.org/10.1016/j.chemosphere.2013.02.066

Zhu Z, Tang X, Ma C et al (2016) Fabrication of conductive and high-dispersed Ppy@Ag/g-C_3N_4 composite photocatalysts for removing various pollutants in water. Appl Surf Sci 387:366–374. https://doi.org/10.1016/j.apsusc.2016.06.124

Zhu W, Sun F, Goei R, Zhou Y (2017a) Facile fabrication of RGO–WO_3 composites for effective visible light photocatalytic degradation of sulfamethoxazole. Appl Catal B Environ 207:93–102. https://doi.org/10.1016/j.apcatb.2017.02.012

Zhu Y, Xue J, Xu T et al (2017b) Enhanced photocatalytic activity of magnetic core–shell Fe_3O_4@Bi_2O_3–RGO heterojunctions for quinolone antibiotics degradation under visible light. J Mater Sci Mater Electron 28:8519–8528. https://doi.org/10.1007/s10854-017-6574-6

Zuo S, Chen Y, Liu W et al (2017) A facile and novel construction of attapulgite/Cu_2O/Cu/g-C_3N_4 with enhanced photocatalytic activity for antibiotic degradation. Ceram Int 43:3324–3329. https://doi.org/10.1016/j.ceramint.2016.11.173

Affiliations

Ankush Majumdar[1] · Anjali Pal[1]

✉ Anjali Pal
anjalipal@civil.iitkgp.ac.in

[1] Department of Civil Engineering, Indian Institute of Technology, Kharagpur, Kharagpur 721302, India